CMS Physics Analysis Summary

Contact: cms-pag-conveners-higgs@cern.ch 2015/08/09

Search for additional neutral Higgs bosons decaying to a pair of tau leptons in pp collisions at $\sqrt{s} = 7$ and 8 TeV

The CMS Collaboration

Abstract

A search for neutral Higgs bosons decaying to tau pairs, beyond the recently discovered boson of mass 125 GeV, is presented. The analysis is based on proton-proton collision data recorded by the CMS experiment in 2011 and 2012, corresponding to an integrated luminosity of 24.6 fb^{-1}, with 4.9 fb^{-1} recorded at 7 TeV and 19.7 fb^{-1} recorded at 8 TeV center-of-mass energy. The search is performed in the context of the minimal supersymmetric extension of the standard model (MSSM). The sensitivity of the analysis is enhanced by performing the search in event categories based on the multiplicity of b-tagged jets and on the transverse momentum of hadronic taus. Hadronic tau decays are identified using a multivariate approach. No evidence for a signal is observed. Exclusion limits in the MSSM parameter space are computed for different MSSM benchmark scenarios: $m_{\mathrm{h}}^{\mathrm{max}}$, $m_{\mathrm{h}}^{\mathrm{mod+}}$, $m_{\mathrm{h}}^{\mathrm{mod-}}$, light-stop, light-stau and τ-phobic. Model independent upper limits on cross section times branching fraction for the neutral Higgs boson production of via gluon fusion and in association with bottom quarks are also given.

1 Introduction

Experimental data from a large number of high energy experiments have overwhelmingly confirmed the predictions of the Standard Model (SM) of fundamental interactions [1–3]. Until recently, an important prediction of the SM, the presence of a neutral scalar, the Higgs boson, lacked experimental confirmation. The Brout-Englert-Higgs mechanism [4–9] is responsible for spontaneously breaking the electroweak symmetry in the SM. By interaction with the Higgs field, the W and Z bosons as well as fermions and in fact also the Higgs boson itself acquires mass. The discovery of a new boson of mass 125 GeV by the CMS and ATLAS collaborations [10, 11] concluded a period of almost 40 years of searches for the SM Higgs boson.

The measured properties of the discovered boson are in agreement with the expectation for the SM Higgs boson in terms of spin, CP quantum numbers, total width and branching fractions for the decay into photons, W and Z bosons, tau leptons and b-quarks [12–15]. However, within the present experimental precision, the discovered boson may as well be one of multiple Higgs bosons, predicted by models with an extended Higgs sector.

Supersymmetry (SUSY) [16, 17], a fundamental symmetry between fermions and bosons, features a particular appealing scalar sector in this context. The scalar sector is strongly constrained and fixed by a few parameters. The mass of the lightest Higgs boson emerges from the theory, and it is protected against the quadratically divergent corrections of the self-energy with respect to a new high energy scale that appear in the case of the SM. For further attractive features of SUSY models see Refs. [18–20].

In the minimal supersymmetric extension of the Standard Model (MSSM) [21, 22] two Higgs doublets give rise to five physical Higgs boson states, two charged Higgs bosons $H^{\pm}$ plus three neutrals: the light and heavy CP-even (scalar) Higgs bosons h and H and the CP-odd (scalar) Higgs boson A. At tree level, the Higgs boson sector of the MSSM is determined by two free parameters, conventionally chosen to be the mass of the pseudo-scalar boson, m_A, and the ratio of vacuum expectation values of the two Higgs doublets, $\tan\beta$.

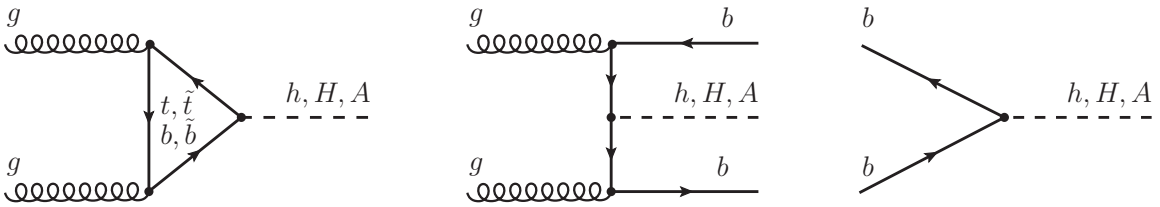

Figure 1: Leading-order diagrams of the gluon fusion (left) and b-quark associated Higgs boson production, in the four-flavor (center) and the five-flavor (right) scheme.

Neutral MSSM Higgs bosons may be produced by two different production mechanisms at the LHC. The gluon fusion process (ggϕ) is the dominant production mode for small and moderate values of $\tan\beta$, while the production in association with b quarks ($bb\phi$) dominates at large values of $\tan\beta$, due to the enhanced Yukawa coupling of the Higgs boson to bottom quarks. We denote by ϕ any of the three neutral MSSM Higgs bosons: h, H or A. Fig. 1 shows the leading order diagrams for neutral MSSM Higgs boson production via gluon fusion and b-quark associated production, the latter in the four-flavour and five-flavour scheme.

The branching fraction for the decay of neutral MSSM Higgs bosons into tau pairs, $\phi \to \tau\tau$, increases in the region of large $\tan\beta$. It also varies as function of m_A. In the m_{A}-$\tan\beta$ region probed by this analysis the branching fraction ranges from 5 to 10%.

The results of a search for additional neutral Higgs bosons, beyond the discovered SM-like Higgs boson of mass 125 GeV, is presented in this paper. The search is based on the full 24.6 fb^{-1} proton-proton collision dataset recorded by the CMS experiment during LHC run 1. The data has been collected at $\sqrt{s} = 7$ TeV and $\sqrt{s} = 8$ TeV center-of-mass energy, corresponding to integrated luminosities of 4.9 fb^{-1} and 19.7 fb^{-1} respectively. Five different $\tau\tau$ signatures are studied: eτ_h, $\mu\tau_h$, $\tau_h\tau_h$, eμ and $\mu\mu$, where we denote by τ_h a hadronic decay of a tau. This search extends previous searches for neutral MSSM Higgs bosons performed by the CMS and ATLAS experiments [23–26], as well as by experiments at the Tevatron [27–30] and at LEP [31].

The results of our search are interpreted in different MSSM benchmark scenarios [32, 33] for pseudoscalar masses between 90 and 1000 GeV, and are used to set model independent limits on cross section times branching fraction, $\sigma(gg\phi) \cdot \mathcal{B}(\phi \to \tau\tau)$ and $\sigma(bb\phi) \cdot \mathcal{B}(\phi \to \tau\tau)$, for gluon fusion and b-quark associated production respectively.

The search presented in this paper supersedes the previous CMS result [25] based on the same dataset. Compared to the previous analysis, the sensitivity of the search presented in this paper is enhanced substantially, by an amount corresponding to an increase in luminosity by about a factor three.

The gain in sensitivity is owed to two major improvements to the analysis: the use of a new algorithm for the identification of τ_h decays [34, 35] and the separation of the candidate events into categories based on τ_h transverse momentum. The τ_h identification discriminant, implemented as an algorithm based on Boosted Decision Trees [36], combines variables related to the isolation and the tau lifetime. Compared with the previous τ_h identification criterion, the new algorithm reduces the mistag rate for jets by about 40%, for the same τ_h identification efficiency. The new categorization exploits the fact that the average transverse momenta of hadronic taus in signal events increases with m_A, while the p_T spectrum of τ_h candidates in background events is expected to be steeply falling. Event categories based on τ_h transverse momentum have been used in the CMS SM Higgs $\to \tau\tau$ analysis [37] for a similar reason. Each improvement increases the expected sensitivity by a similar amount. The sensitivity of the search for additional neutral Higgs bosons in the $\tau\tau$ decay channel presented in this paper is enhanced in particular in the region of high mass, which for the most part is yet unexplored.

2 CMS detector

The central feature of the CMS apparatus is a superconducting solenoid of 6 m internal diameter, providing a magnetic field of 3.8 T. Within the superconducting solenoid volume are a silicon pixel and strip tracker, a lead tungstate crystal electromagnetic calorimeter (ECAL), and a brass and scintillator hadron calorimeter (HCAL), each composed of a barrel and two endcap sections. Muons are measured in gas-ionization detectors embedded in the steel flux-return yoke outside the solenoid. Extensive forward calorimetry complements the coverage provided by the barrel and endcap detectors. The first level (L1) of the CMS trigger system, composed of custom hardware processors, uses information from the calorimeters and muon detectors to select the most interesting events in a fixed time interval of less than 4 μs. The high level trigger (HLT) processor farm further decreases the event rate from around 100 kHz to around 400 Hz, before data storage. A more detailed description of the CMS detector, together with a definition of the coordinate system used and the relevant kinematic variables, can be found in Ref. [38].

3 Data samples and Monte Carlo simulation

The search is based on datasets recorded by the CMS experiment at center-of-mass energies of $\sqrt{s} = 7$ TeV and $\sqrt{s} = 8$ TeV in 2011 and 2012 respectively. The data analyzed by the $e\tau_h$, $\mu\tau_h$, $e\mu$ and $\mu\mu$ channels corresponds to an integrated luminosity of 4.9 fb^{-1} at $\sqrt{s} = 7$ TeV plus 19.7 fb^{-1} at $\sqrt{s} = 8$ TeV. In the $\tau_h\tau_h$ channel, the search is based on 18.3 fb^{-1} of data collected at $\sqrt{s} = 8$ TeV.

Simulated samples of $gg \to \phi$ and $gg \to \phi b$ signal events have been generated by PYTHIA [39] and are used to determine acceptance times efficiency of the analysis for MSSM Higgs bosons of different mass. In particular for MSSM Higgs bosons of low mass, the signal acceptance depends on the Higgs p_T spectrum to some extent. Generated $gg \to \phi$ events are reweighted to the Higgs p_T distribution computed at NLO precision using POWHEG [40], which accounts for the finite mass of bottom and top quarks in the calculation of the loop diagram Fig. 1. We evaluate the loop diagram for a mixture in equal proportions of bottom and top quark loops and treat the difference as a systematic uncertainty.

Cross sections and branching fractions for different MSSM benchmark scenarios are provided by the LHC Higgs Cross Section Working Group [41]. The cross sections for the gluon fusion process have been computed using SUSHI [42], for all MSSM benchmark scenarios except for the m_h^{max} scenario. The SUSHI calculation includes SUSY NLO QCD corrections [43–47] plus electroweak corrections due to light-fermion loop effects [48, 49]. The gluon fusion cross section for the m_h^{max} scenario are obtained from HIGLU [50, 51]. The cross sections for the production of neutral MSSM Higgs bosons in association with b-quarks have been computed by combining the four-flavor NLO QCD calculation [52, 53] and the five-flavor NNLO QCD calculation, as implemented in BBH@NNLO [54]. The combination is performed using the Santander matching scheme [55]. The Higgs boson Yukawa couplings used in all cross section calculations have been obtained from FEYNHIGGS [56–59]. The branching fractions for the Higgs boson decay to taus in the different MSSM benchmark scenarios have been computed using FEYNHIGGS and HDECAY [60–62], as described in Ref. [63].

Backgrounds arising from $Z/\gamma^* \to ee$, $Z/\gamma^* \to \mu\mu$, W+jet, $t\bar{t}$, single top and di-boson (WW, WZ, ZZ) production are modeled using the Monte Carlo simulation. The $Z/\gamma^* \to \ell\ell$ (ℓ = e, μ), W+jet, $t\bar{t}$ and di-boson samples are generated by MADGRAPH [64], the single top samples by POWHEG [40]. Samples binned in jet multiplicity on parton level are used for the $Z/\gamma^* \to \ell\ell$ and W+jets backgrounds in the 8 TeV analysis, in order to enhance the background event statistics in regions of high signal purity. The $Z/\gamma^* \to \ell\ell$ and W+jet samples are normalized according to cross sections computed at NNLO accuracy [65]. The top pair production cross section measured by CMS [66] is used to normalize the $t\bar{t}$ sample. A reweighting is applied to generated $t\bar{t}$ events in order to improve the modeling of the top quark p_T spectrum measured in data [67–69]. The cross sections for single top and di-boson production have been computed at NLO accuracy [70]. QCD multijet background is determined entirely from data.

Standard model Higgs boson production via gluon fusion, vector boson fusion as well as by associated production of the Higgs with W and Z bosons and with $t\bar{t}$ pairs is modeled using POWHEG. The samples have been produced for a Higgs mass of $m_H = 125$ GeV and are normalized according to the cross sections and branching fractions given in Ref. [41] for $m_H = 125$ GeV.

All Monte Carlo samples are produced using PYTHIA, with the tune $Z2^*$ [71], to model parton shower and hadronization processes. Taus are decayed by TAUOLA [72]. The CTEQ6L1 (CTEQ6M) [73] parton distributions functions are used in case of the Monte Carlo samples

produced by PYTHIA or MADGRAPH (POWHEG).

On average 9 (21) inelastic proton-proton interactions, referred to as pileup, occured per LHC bunch crossing in 2011 (2012). Minimum bias events generated by PYTHIA are added to all Monte Carlo simulated events according to the pileup profile of the analyzed data.

All generated events are passed through a detailed simulation of the CMS apparatus, based on GEANT [74], and are reconstructed using the same version of the CMS event reconstruction software as the data.

4 Event reconstruction

The information provided by all CMS subdetectors is employed by a particle-flow (PF) algorithm [75–78] to identify and reconstruct individual particles in the event, namely muons, electrons, photons, charged and neutral hadrons. These particles are then used to reconstruct jets, τ_h candidates and the missing transverse energy vector $\vec{E}_T^{miss}$, as well as to quantify the isolation of leptons.

Electrons are reconstructed by matching tracks reconstructed in the inner detector to energy deposits in the ECAL [75, 79]. A dedicated algorithm [80] that accounts for the emission of Bremsstrahlungs-photons is used to reconstruct the tracks of electron candidates. Energy loss due to Bremsstrahlung is reconstructed by searching for energy deposits in the ECAL located in direction tangent to the electron track. A multivariate (MVA) approach based on boosted decision trees (BDTs) [36] is employed for electron identification [81]. Observables that quantify the quality of the electron track, the compactness of the electron cluster in direction transverse and longitudinal to the electron direction, and the matching between track momentum and direction with the sum and position energy deposits in the ECAL are used as inputs to the BDT. The electron energy scale is calibrated using $J/\Psi \to ee$, $\Upsilon \to ee$ and $Z \to ee$ decays. Additional requirements are applied in order to reject electrons originating from photon conversions.

The identification of muons is based on linking track segments reconstructed in the silicon tracking detector and in the muon system [82]. The matching between track segments is done outside-in, starting from a track in the muon system, and inside-out, starting from a track reconstructed in the inner detector. In case a link can be established, the track parameters are refitted using the combination of hits in the inner and outer detectors and the track is referred to as global muon track. Quality cuts are applied on the multiplicity of hits, on the number of matched segments and on the quality of the global muon track fit, quantified by χ^2.

Electrons and muons in signal events are expected to be isolated, while leptons originating from heavy flavour (charm and bottom quark) decays as well as in-flight decays of pions and kaons are typically found within jets. Lepton isolation hence provides a useful handle to discriminate the signal from the QCD background. The isolation is computed with respect to charged particles, photons plus neutral hadrons reconstructed by the PF algorithm. Details, including the procedure employed to correct for pileup, are given in Ref. [25].

Hadronic tau decays are reconstructed by the *hadrons plus strips* (HPS) algorithm [34, 35, 83]. The algorithm allows to reconstruct individual hadronic decay modes of the tau: $\tau^- \to h^-\nu_\tau$, $\tau^- \to h^-\pi^0\nu_\tau$, $\tau^- \to h^-\pi^0\pi^0\nu_\tau$ and $\tau^- \to h^-h^+h^-\nu_\tau$, where $h^\pm$ denotes either a charged pion or kaon. The decay modes of τ^+ are the charge conjugate of the τ^- decay modes. Hadronic tau candidates are built by combining the charged hadrons reconstructed by the PF algorithm with neutral pions. The neutral pions are reconstructed by clustering the photons reconstructed by the PF algorithm within rectangular strips that are narrow in η-, but wide in ϕ-direction, to ac-

count for the broadening of energy deposits in the ECAL in case one of the photons produced in $\pi^0 \to \gamma\gamma$ decays converts within the tracking detector. Due to the all silicon tracking detector of CMS, the probability for photon conversions is sizeable. For this reason, the electrons reconstructed by the PF algorithm are considered in the reconstruction of the neutral pions too. The main handle to separate hadronic tau decays from quark and gluon jets is to apply tight isolation requirements. The cut-based tau isolation discriminators with pileup corrections described in Ref. [35] are used to identify hadronic tau decays in case of the 7 TeV data. In case of the 8 TeV data, the MVA-based tau identification algorithm described in Ref. [35] is used. The isolation of the τ_h candidates is complemented by observables that provide sensitivity to the lifetime of the tau. The transverse impact parameter of the "leading" (highest p_T) track of the τ_h candidate with respect to the primary collision vertex is used for τ_h candidates reconstructed in any decay mode. In case the τ_h candidate is reconstructed in the decay mode $\tau^- \to h^-h^+h^-\nu_\tau$, a fit of the three tracks to a common secondary vertex is attempted and the distance to the primary collision vertex is used as additional input variable to the MVA. Further details are given in Ref. [35]. Additional discriminators are employed to separate hadronic tau decays from electrons and muons.

Collision vertices are reconstructed by the deterministic annealing algorithm [84, 85]. The reconstructed vertex position is required to be compatible with the location of the LHC beam in the x-y plane. The primary collision vertex is taken to be the vertex for which the quantity $\sum_{tracks} p_T^2$ is maximal. The sum extends over all tracks associated to a given vertex. Electrons, muons and hadronic taus are required to be compatible with originating from the primary collision vertex.

Jets within the range $|\eta| < 4.7$ are reconstructed by the anti-k_T algorithm [86] with a distance parameter $R = 0.5$. Reconstructed jets are required not to overlap with identified electrons, muons or hadronic taus within $\Delta R < 0.5$ and to pass two levels of jet identification criteria: Fake jets, mainly arising from calorimeter noise, are rejected by requiring reconstructed jets to pass a set of loose jet identification criteria [87]. Jets originating from pileup interactions are rejected by an MVA-based jet identification discriminator, based on vertex and jet shape information [88]. The energy of reconstructed jets is calibrated as function jet p_T and η [89]. Fastjet-ρ-based [90, 91] jet energy corrections are applied in order to compensate for pileup effects. Jets originating from the hadronization of b quarks are identified by the *combined secondary vertex* (CSV) algorithm [92], which exploits observables related to the long lifetime of b hadrons and to the higher particle multiplicity and mass of b-jets compared to light quark and gluon jets.

The missing transverse energy in the event, $E_\mathrm{T}^\mathrm{miss}$, is reconstructed using a multivariate regression algorithm [93]. The algorithm utilizes the fact that pileup predominantly produces jets of low p_T, while leptons and high p_T jets are almost exclusively produced by the hard-scattering processes, to reduce the effect of pileup on the $E_\mathrm{T}^\mathrm{miss}$ resolution.

The Higgs boson signal is distinguished from backgrounds by means of the tau-lepton pair invariant mass, $m_{\tau\tau}$, reconstructed by a likelihood based algorithm [23, 94]. The resolution on $m_{\tau\tau}$ achieved by the algorithm typically amounts to 20% relative to the true mass of the tau pair. Distributions of $m_{\tau\tau}$ reconstructed in simulated $\mathrm{Z}/\gamma^* \to \tau\tau$ background events and for hypothetical MSSM Higgs$\to \tau\tau$ signals of $m_\mathrm{A} = 120$, 200 and 300 GeV are shown in Fig. 2. The events are selected in the $\mu\tau_\mathrm{h}$ channel. The visible mass of muon plus hadronic tau, m_{vis}, is shown for comparison. The reconstruction of the tau-lepton pair invariant mass is seen to improve the separation of the Higgs$\to \tau\tau$ signal from the $\mathrm{Z}/\gamma^* \to \tau\tau$ background.

Two further observables are reconstructed in order to improve the separation of the signal from

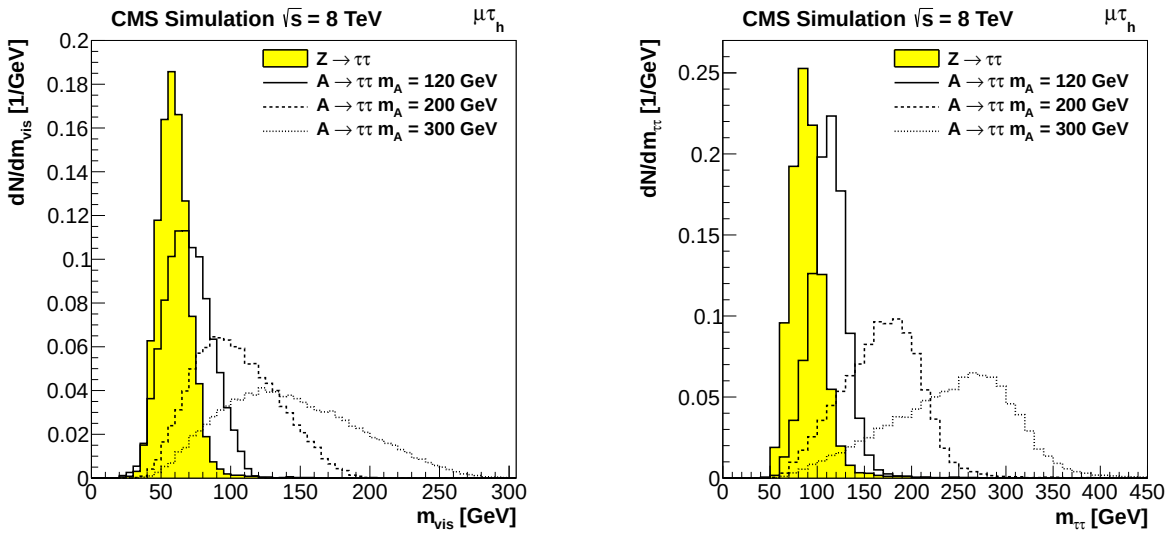

Figure 2: Distribution of visible mass (left) and tau-lepton pair invariant mass (right) in simulated $Z/\gamma^* \rightarrow \tau\tau$ background events and for hypothetical MSSM Higgs $\rightarrow \tau\tau$ signals of $m_A = 120$, 200 and 300 GeV. The events are selected in the $\mu\tau_h$ channel.

backgrounds, in particular from those arising from W+jet and $t\bar{t}$ production.

The transverse mass, m_T, of electron (muon) plus missing transverse energy is used to remove the W+jets background in the $e\tau_h$ ($\mu\tau_h$) channel. The transverse mass is defined by:

$$m_T = \sqrt{2\, p_T^{\ell}\, E_T^{miss}\ (1 - \cos\Delta\phi)}, \tag{1}$$

where the symbol ℓ refers to the electron (muon) and $\Delta\phi$ denotes the difference in azimuthal angle between the lepton momentum and the missing transverse energy vector $\vec{E}_T^{miss}$.

Background due to $t\bar{t}$ production in the $e\mu$ channel is reduced by means of a topological discriminator [95], which is based on computing the projections:

$$P_\zeta = \left(\vec{p}_T^{\,e} + \vec{p}_T^{\,\mu} + \vec{E}_T^{miss}\right) \cdot \frac{\vec{\zeta}}{|\vec{\zeta}|} \qquad \text{and} \qquad P_\zeta^{vis} = \left(\vec{p}_T^{\,e} + \vec{p}_T^{\,\mu}\right) \cdot \frac{\vec{\zeta}}{|\vec{\zeta}|} \tag{2}$$

on the axis $\vec{\zeta}$, given by the bisector of the electron and muon momenta in the transverse plane. The discriminator relies on the fact that the angle between the neutrinos produced in tau decays and the visible tau decay products is typically small, resulting in the missing transverse energy vector in signal events to point in direction of the visible tau decay products, while this is often not the case in $t\bar{t}$ background events. Events satisfying $P_\zeta - 1.85 \cdot P_\zeta^{vis} > -20$ GeV are considered signal-like.

5 Event selection

The events used in this search have been recorded by dedicated triggers that use a combination of electron, muon and hadronic tau trigger objects [82, 96, 97]. The identification criteria and transverse momentum thresholds of these objects were progressively tightened as the LHC instantaneous luminosity increased over the data-taking period.

The eτ_h and $\mu\tau_h$ channels utilize triggers based on the presence of an electron+τ_h or muon+τ_h pair to record the events. Events selected in the 2011 (2012) data are required to contain an electron of $p_T > 20$ (24) GeV or a muon of $p_T > 17$ (20) GeV and $|\eta| < 2.1$ plus a τ_h candidate of $p_T > 30$ GeV and $|\eta| < 2.3$. Electrons and muons are required to pass tight isolation requirements, $I_\ell < 0.10 \cdot p_T^\ell$, computed as described in Ref. [25]. Hadronic tau candidates selected in the 2011 (2012) data are required to pass a cut $I_\tau < 1.5$ GeV on the raw output of the cutoff-based discriminator (to pass the medium working-point of the MVA-based tau identification discriminator) and to be of opposite charge to the electron or muon. The hadronic tau candidates selected in the eτ_h ($\mu\tau_h$) channel are further required to pass tight (loose) electron veto and loose (tight) muon veto criteria. The transverse mass of electron (muon) plus missing transverse energy, computed according to Eq. 1, is required to satisfy $m_T < 30$ GeV. Events containing additional electrons or muons of $p_T > 15$ GeV and $|\eta| < 2.4$, passing loose identification and isolation criteria, are rejected, in order to remove $Z/\gamma^* \to ee$, $Z/\gamma^* \to \mu\mu$ and di-boson backgrounds.

Events in the $\tau_h\tau_h$ channel have been recorded by a combination of triggers based on the presence of two hadronic taus in the event and by single jet triggers. The double-tau trigger has been operational during most of the 2012 data-taking period and collected data corresponding to an integrated luminosity of 18.3 fb^{-1}. It reaches its maximum efficiency of about 85% per tau for hadronic taus of p_T greater than 60 GeV. A single jet triggers with a p_T threshold of 320 GeV is utilized to record events in which the τ_h candidate of higher p_T has a transverse momentum above 350 GeV. Selected events are required to contain two τ_h candidates of $p_T > 45$ GeV, $|\eta| < 2.1$ and opposite charge, reconstructed by the HPS algorithm and passing the medium working-point (WP) of the MVA-based tau identification discriminator. The τ_h candidate of lower p_T is further required to pass selection criteria that separate hadronic tau decays from electrons. Events containing electrons or muons of $p_T > 15$ GeV and $|\eta| < 2.4$, passing loose identification and isolation criteria, are rejected to avoid overlap with the eτ_h and $\mu\tau_h$ channels.

The $\mu\mu$ (eμ) channel employs single and double-muon triggers (triggers based on the presence of an electron+muon pair). Electrons (muons) are selected within the geometric acceptance $|\eta| < 2.3$ ($|\eta| < 2.1$). The lepton of higher (lower) p_T is required to satisfy $p_T > 20$ (10) GeV. Muons selected in the $\mu\mu$ channel are required to pass tight isolation criteria, $I_\mu < 0.10 \cdot p_T^\mu$. In the e$\mu$ channel, electrons and muons of $|\eta| < 1.479$ ($|\eta| > 1.479$) are required to pass an isolation criterion of $I_\ell < 0.10 \cdot p_T^\ell$ ($I_\ell < 0.15 \cdot p_T^\ell$). The large background arising from $Z/\gamma^* \to \mu\mu$ events in the $\mu\mu$ channel is reduced by a multivariate discriminator, based on different muon kinematic variables and the distance of closest approach between the two muon tracks. In the eμ channel the background due to $\bar{t}t$ production is removed by a cut $P_\zeta - 1.85 \cdot P_\zeta^{vis} > -20$ GeV on the topological discriminator given by Eq. 2.

6 Event categorization

The events selected are gathered for further analysis in two categories based on the presence or not of a b-tagged jet. The two event categories provide sensitivity to the different production mechanism ggϕ and $bb\phi$. The overall sensitivity of the analysis increases too, due to the fact that the signal-to-background ratio is more favorable in events containing b-tagged jets. Events considered in the *b-tag* category are required to contain at least one jet of $p_T > 20$ GeV and $\eta < 2.4$, passing the medium WP of the CSV b-tagging algorithm described in section 4), and at most one jet of $p_T > 30$ GeV, including the b jet. The latter requirement suppresses $\bar{t}t$ background. The events selected in the *no-b-tag* category are required to contain no b-tagged jet of $p_T > 20$ GeV and $\eta < 2.4$.

In case of the $e\tau_h$, $\mu\tau_h$ and $\tau_h\tau_h$ channels in the 8 TeV data the *b-tag* (*no-b-tag*) category is split into two (three) subcategories, defined by the transverse momentum of the hadronic tau in the event. In case of the $\tau_h\tau_h$ channel, the subcategories are defined using the transverse momentum of the hadronic tau of lower p_T. This represents a further splitting of the categories defined in the previous CMS MSSM Higgs $\to \tau\tau$ analysis [25]. The expected sensitivity to MSSM Higgs bosons is improved by about 20%, due to the fact that the signal to background ratio varies along the subcategories. The performance of the new categorization is expected to be larger for searches at small hypothesized Higgs boson masses. For higher masses ($m_\phi \gtrsim 400$ GeV), the improved categorization has a small effect on the expected sensitivity because most of the events present high transverse momentum hadronic taus ($p_T \gtrsim 80$ GeV), and hence will not be distributed to several subcategories. The p_T thresholds that define the subcategories, given in Tab. 1, are chosen such that the event statistics in each of the subcategories is sufficient to obtain smooth $m_{\tau\tau}$ shape templates for the dominant background processes.

Channel	no-b-tag		
	low	medium	high
$e\tau_h$	$30 < p_T < 45$ GeV	$45 < p_T < 60$ GeV	$p_T > 60$ GeV
$\mu\tau_h$	$30 < p_T < 45$ GeV	$45 < p_T < 60$ GeV	$p_T > 60$ GeV
$\tau_h\tau_h$	$45 < p_T < 60$ GeV	$60 < p_T < 80$ GeV	$p_T > 80$ GeV

Channel	b-tag	
	low	high
$e\tau_h$	$30 < p_T < 45$ GeV	$p_T > 45$ GeV
$\mu\tau_h$	$30 < p_T < 45$ GeV	$p_T > 45$ GeV
$\tau_h\tau_h$	$45 < p_T < 60$ GeV	$p_T > 60$ GeV

Table 1: Definition of subcategories in terms of τ_h candidate transverse momentum, used to analyze events selected in the $e\tau_h$, $\mu\tau_h$ and $\tau_h\tau_h$ channels in case of the 8 TeV data.

For the purpose of background studies, we define as "inclusive" event category the conjunction of *b-tag* and *no-b-tag* categories, including all subcategories based on hadronic tau p_T.

7 Background estimation

The shapes and yields of the major backgrounds in each of the channels are obtained from data.

The Drell-Yan production of tau pairs, $Z/\gamma^* \to \tau\tau$, represents the dominant source of background in the $e\tau_h$, $\mu\tau_h$ and $e\mu$ channels. The irreducible $Z/\gamma^* \to \tau\tau$ background is modeled via the "embedding" technique. The method is based on selecting $Z/\gamma^* \to \mu\mu$ events in data and replacing the reconstructed muons by generator level tau leptons. The taus are decayed using TAUOLA. Tau polarization effects are modeled using TAUSPINNER [98]. The GEANT based detector simulation is used to model the detector response to the tau decay products. Tracks in the inner detectors, energy deposits in the calorimeter plus hits in the muon system that are due to the tau decay products are mixed with the remains of the $Z/\gamma^* \to \mu\mu$ event after all detector signals of the two muons originating from the Z boson decay have been removed. The event is then reconstructed and analyzed as if it were real data. The method substantially reduces the systematic uncertainties due to jet energy scale, E_T^{miss} resolution and on uncertainties related to the modeling of *b*-jets. Embedded samples have been produced for the full LHC run 1 data-taking period. The normalization and shape of the $Z/\gamma^* \to \tau\tau$ background estimate obtained from the embedding method is corrected for the contamination of the em-

bedded samples by non-Drell-Yan backgrounds, predominantly $\mathrm{t\bar{t}}$, that arises from impurities of the $Z/\gamma^* \to \mu\mu$ event sample selected in data. These corrections are obtained by applying the embedding procedure on simulated samples of these backgrounds, and then subtracting their expected contribution to the embedded data samples.

The Drell-Yan production of muon pairs constitutes the main background in the $\mu\mu$ channel. The yield of the $Z/\gamma^* \to \mu\mu$ background is obtained by fitting the distribution of the distance of closest approach between the tracks of the two muons, observed in a control region, with shape templates for prompt muons and for muons originating from tau decays. The fit is performed in bins of the visible mass, m_{vis}, of the two muons. The contributions of QCD, W+jets, $\mathrm{t\bar{t}}$, single top and di-boson backgrounds are subtracted from the data before performing the fit. The shape of the $m_{\tau\tau}$ distribution for the $Z/\gamma^* \to \mu\mu$ background in a given bin of m_{vis} in the $\mu\mu$ channel is obtained from the Monte Carlo simulation. The Drell-Yan production of electron pairs is relevant for the $e\tau_h$ channel. The background contribution is typically due to events in which an electron is misidentified as hadronic tau decay. Shape and normalization of this background are obtained from the Monte Carlo simulation. The yield of $Z/\gamma^* \to ee$ events is corrected by the $e \to \tau_h$ misidentification rate measured in data via the "tag-and-probe" technique [35]. The contribution of $Z/\gamma^* \to \mu\mu$ background to the $\mu\tau_h$ channel is insignificant, due to the small rate of $\mu \to \tau_h$ fakes.

The W+jets background contributes predominantly to the $e\tau_h$ and $\mu\tau_h$ channels. In typical events, the W boson decays into an electron or muon and a jet is misidentified as hadronic tau. The shape of the W+jets background is obtained by selecting events passing relaxed tau identification criteria and weighting the events by the probability for jets to pass the nominal tau identification discriminator, measured as function of p_T and η of the τ_h candidate in the data. The normalization is also determined from data, using a control region dominated by W+jets background, obtained by inverting the cut on the transverse mass and requiring $m_T > 70$ GeV. The control region is referred to as *high-m_T sideband*. The event yield observed in the high-m_T sideband is corrected for the contribution of other backgrounds and then extrapolated into the signal region, using an extrapolation factor obtained from the Monte Carlo simulation. By means of this procedure, the W+jets background yield is determined separately for the $e\tau_h$ and $\mu\tau_h$ channels and each event category. In case of the *b-tag* event categories the b-tagging criteria are relaxed, in order to increase the event statistics of the shape templates.

QCD multijet events in which two quark or gluon jets get misidentified as hadronic tau decays constitute the dominant background in the $\tau_h\tau_h$ channel. The background is estimated by selecting events containing two τ_h candidates of opposite charge (OS events) in which the "leading" (higher p_T) τ_h candidate passes the nominal and the "subleading" (lower p_T) τ_h candidate passes relaxed, but fails the nominal tau identification criteria. Events selected in the OS control region are weighted by the ratio of the probability for jets to pass the nominal to the probability for jets to pass relaxed, but fail the nominal tau identification criteria. The ratio is measured as function of jet p_T and η in events containing two τ_h candidates of the same charge (SS events). Small contributions of other backgrounds to the OS and SS control regions are subtracted using the simulation. The QCD yield and normalization is determined separately for each event category in the signal region, by applying the corresponding category selection criteria to the events in the OS control region. In case of the *b-tag low* and *b-tag high* event categories, the normalization (shape) is obtained with nominal (relaxed) b-tagging criteria applied.

In the $e\tau_h$ and $\mu\tau_h$ channels, the contribution of QCD multijet background is typically due to events in which the reconstructed τ_h candidate is due to misidentified quark or gluon jet. Reconstructed muons typically originate from the decay of a heavy (charm or bottom) quark,

while reconstructed electrons may either originate from the decay of a heavy quark or be due to a misidentified pion or kaon. The contribution of QCD multijet background to these channels is estimated by selecting events in which the hadronic tau candidate and the electron or muon are of the same charge. Contributions of Drell-Yan and W+jets backgrounds to the SS control region are determined as described above and subtracted. The $\mathrm{t\bar{t}}$, single top and di-boson backgrounds are subtracted based on simulation. The QCD multijet background yield in the signal region is estimated by scaling the event yield observed in the SS control region by a factor of 1.06, the ratio of OS to SS events measured in a pure QCD multijet sample that has been obtained by inverting the isolation requirements for electrons and muons and relaxing the hadronic tau identification criteria. The procedure is applied separately for each event category. In case of the *b-tag* event categories, relaxed *b*-tagging criteria are applied, in order to increase the event statistics of the shape templates.

The small background due to W+jets and QCD multijet production in the eμ channel is due to events in which one or two jets are misidentified as leptons. The background is estimated using control regions in which one lepton passes the nominal, while the other lepton passes relaxed, but fails the nominal selection criteria. Extrapolation factors from the control region to the signal region are measured in an independent event sample dominated by QCD multijet events. The contribution of backgrounds with genuine electron plus muon pairs to the control regions is subtracted based on the simulation.

The production of top pairs is one of the main backgrounds in the eμ channel as well as in the *b-tag* categories of other channels. The shape of the $\mathrm{t\bar{t}}$ background is obtained from the Monte Carlo simulation. The normalization is determined using a control sample of eμ events with two *b*-tagged jets.

The small contribution of the di-boson and single top backgrounds is estimated based on simulation.

8 Systematic uncertainties

Various imprecisely known or simulated effects can alter the shape and normalization of the tau-lepton pair invariant mass spectrum used to infer the presence or absence of a signal.

Electron and muon trigger, identification and isolation efficiencies have been measured using $\mathrm{Z}/\gamma^* \to \mathrm{ee}$ and $\mathrm{Z}/\gamma^* \to \mu\mu$ events via the tag-and-probe method [82, 99] with an accuracy of 2%. The efficiency to reconstruct and identify hadronic tau decays has been measured using $\mathrm{Z}/\gamma^* \to \tau\tau$ events with an uncertainty of 6% [35]. An additional uncertainty of $0.02\% \cdot p_T^\tau$ [GeV] on the hadronic tau identification efficiency accounts for the extrapolation from the Z boson resonance to higher p_T, including the uncertainty on the rate with which the charge of high p_T taus is mismeasured. The uncertainty on the tau trigger efficiency amounts to 3% in the $e\tau_\mathrm{h}$ and $\mu\tau_\mathrm{h}$ channel and to 4.5% per tau in the $\tau_\mathrm{h}\tau_\mathrm{h}$ channel.

Uncertainties on the jet energy scale (JES) affect the probability to enter different event categories. The JES has been validated using γ+jets, Z+jets and QCD di-jet events [89]. The uncertainty on the JES ranges from 1-10%, depending on jet p_T and η. The effect of jet energy resolution uncertainties on the analysis is negligible. The efficiency for *b*-jets to pass the medium WP of the CSV *b*-tagging algorithm and the mistag rates for light quark and gluon jets have been measured in $\mathrm{t\bar{t}}$ and QCD multijet events and are in the range 2-7% and 10-20% respectively [92, 100].

The yield of $\mathrm{Z}/\gamma^* \to \mathrm{ee}$ and $\mathrm{Z}/\gamma^* \to \mu\mu$ backgrounds is affected by the uncertainty on the

rate with which electrons and muons get misidentified as hadronic tau decays. The $e \to \tau_h$ ($\mu \to \tau_h$) misidentification rate in $Z/\gamma^* \to ee$ ($Z/\gamma^* \to \mu\mu$) events has been measured with an accuracy of 20% (30%) using the tag-and-probe method [35].

The uncertainty on the integrated luminosity amounts to 2.2% in case of the 7 TeV data [101] and to 2.6% for the 8 TeV data [102].

The uncertainty on the cross section of background processes amount to 5% in case of the Drell-Yan electron pair and muon pair background and to 15% for the di-boson and single top backgrounds. The quoted uncertainties include the theoretical uncertainty on the cross section calculation, the uncertainty on the parton distribution functions (PDF), estimated following the recommendation in Ref. [103], plus the uncertainness on the modeling of parton showers and of the underlying event.

The SM Higgs yield is assigned an uncertainty of 30%, reflecting the present experimental uncertainty on the signal rate measured by the CMS and ATLAS SM Higgs $\to \tau\tau$ analyses [37, 104].

The uncertainty on the reweighting of the $t\bar{t}$ sample generated by MADGRAPH according to generator level top quark p_T, described in section 3, is estimated by varying the weights between no and twice the nominal correction being applied.

Uncertainties on the energy scale of leptons have an effect on the rate and on the shape of signal and background processes. The energy scale of electrons and muons has been calibrated using $J/\Psi \to \ell\ell$, $\Upsilon \to \ell\ell$ and $Z/\gamma^* \to \ell\ell$ (ℓ = e, μ) events and is known with an uncertainty of 1%. The hadronic tau energy scale (τ-ES) has been measured in $Z/\gamma^* \to \tau\tau \to \mu\tau_h$ events, by comparing the distribution of τ_h candidate mass and of the visible mass of muon plus hadronic tau between data and Monte Carlo simulation. The events used for the τ-ES measurement overlap with the event sample selected in the $\mu\tau_h$ channel of this analysis. We conservatively assign 3% uncertainty to the τ-ES. It has been checked that the choice of the τ-ES uncertainty has little effect on the final results. The maximum likelihood fit described in section 9 constrains the nuisance parameter for the τ-ES to a confidence interval of width $\mathcal{O}(0.5\%)$.

The E_T^{miss} resolution is known with few percent uncertainty from studies performed in $Z/\gamma^* \to \mu\mu$, $Z/\gamma^* \to ee$ and γ+jets events. The effect on the shape of the $m_{\tau\tau}$ distribution is small. The uncertainty on the E_T^{miss} resolution mainly affects the $e\tau_h$ and $\mu\tau_h$ channels, due to the $m_T < 30$ GeV cut.

The uncertainties discussed so far apply to the neutral MSSM Higgs boson signal, SM Higgs $\to \tau\tau$ production and to all backgrounds that are obtained from the Monte Carlo simulation: $Z/\gamma^* \to \ell\ell$ (ℓ = e, μ), di-boson and single top production.

The backgrounds determined from data are subject to rate and shape uncertainties. The uncertainty on the yield of the QCD multijet background in the $e\tau_h$, $\mu\tau_h$ and $\tau_h\tau_h$ channel amounts to 10% in *no-b-tag* and to 20% in *b-tag* categories. In the $e\mu$ and $\mu\mu$ channels, the uncertainty on the (small) QCD background contribution ranges from 10-30%, depending on the event category. Additional uncertainties on the shape of the QCD background are included in the $e\tau_h$, $\mu\tau_h$, $\tau_h\tau_h$ and $e\mu$ channels. The rate of W+jets background in the $e\tau_h$ and $\mu\tau_h$ channels is known with an uncertainty of 10% (30%) in the *no-b-tag* (*b-tag*) categories. The quoted uncertainties include the uncertainness on the extrapolation factor from the high-m_T sideband to the signal region and the statistical uncertainty on the number of events observed in the high-m_T sideband. Additional uncertainties on the shape of the W+jets background are included. The normalization of the $t\bar{t}$ background is determined with an uncertainty of 10%. The yield of the Drell-Yan muon

pair production background in the $\mu\mu$ channel has an uncertainty of 5%.

The $Z/\gamma^* \to \tau\tau$ background, modeled via the embedding technique, is subject to lepton reconstruction, identification and trigger efficiency uncertainties plus the uncertainties on electron, muon and hadronic tau energy scales.

The theoretical uncertainties on the MSSM Higgs signal cross sections vary with m_A, $\tan\beta$ and the benchmark scenario considered, and ranges from 10-25%. The MSTW2008 [105] PDF set has been used for computing the cross sections, and PDF related uncertainties have been estimated according to the prescription given in Ref. [106]. The renormalization and factorization scales used in the theoretical calculations and the variation considered are summarized in Ref. [41].

An additional uncertainty on signal acceptance times efficiency arises from the uncertainty on the p_T spectrum of neutral MSSM Higgs bosons produced via gluon fusion. While the p_T of the Higgs boson is not used in the analysis directly, it affects the p_T distribution of the electrons, muons and hadronic taus produced in the decay of the Higgs boson. The uncertainty is estimated by taking the difference between signal acceptance times efficiency computed for the case that the gluon fusion diagram in Fig. 1 is dominated by bottom quark ($\tan\beta = 30$) and by top quark ($\tan\beta = 2$) loops respectively. The effect is found to be of moderate size for $m_A \lesssim 300$ GeV and small for $m_A \gtrsim 300$ GeV. The increase of theoretical uncertainties on the calculation of the Higgs boson p_T spectrum at high $\tan\beta$ is estimated by varying the b quark resummation scale between 25 GeV and 100 GeV and taking the difference as additional systematic uncertainty. The effect of possible loop contributions of squarks and sleptons has been estimated by comparing the p_T spectra computed for different MSSM benchmark models. It is found to be small compared to the difference between bottom quark and top quark loops and not considered in this analysis.

9 Statistical analysis

Evidence for the decay of the observed SM-like Higgs boson of mass 125 GeV into taus, published recently by CMS and ATLAS [37, 104], motivates a careful definition of the *signal+background* and *background-only* hypotheses. In this section we describe in detail how we distinguish a MSSM Higgs $\to \tau\tau$ signal from SM Higgs $\to \tau\tau$ decays plus backgrounds.

The presence or absence of a neutral MSSM Higgs boson signal is inferred via a binned maximum likelihood fit to the observed distribution of tau-lepton pair invariant mass, that is used as *discriminant variable* in the $e\tau_h$, $\mu\tau_h$, $\tau_h\tau_h$ and $e\mu$ channels. In the $\mu\mu$ channel, the sensitivity of the search is enhanced by fitting the two-dimensional distribution of $m_{\tau\tau}$ versus m_{vis}, the visible mass of the two muons, taking advantage of the fact that most of the large Drell-Yan muon pair production background contributing to this channel is concentrated within a narrow peak around the Z-boson mass in the m_{vis} distribution. The fit is performed jointly across the five channels $e\tau_h$, $\mu\tau_h$, $\tau_h\tau_h$, $e\mu$ and $\mu\mu$ and all event categories. It includes the 7 TeV as well as the 8 TeV data unless explicitly stated otherwise.

The likelihood function $\mathcal{L}$ used in the fit is given by the product of Poisson probabilities to observe n_i events in each bin i of the discriminant variable distributions:

$$\mathcal{L}(\mu,\theta) = \mathcal{P}(\text{ data }|\mu,\theta)\cdot p(\tilde{\theta}|\theta) = \prod_i \frac{\nu_i^{n_i}}{n_i!}\exp(-\nu_i)\cdot p(\tilde{\theta}|\theta). \quad (3)$$

The number of events expected in the i-th bin, ν_i, depends on the *signal strength modifier* μ that

quantifies the rate of the signal and on the values of nuisance parameters, θ, which represent the systematic uncertainties discussed in section 8.

The function $p(\tilde{\theta}|\theta)$ represents the probability to observe a value $\tilde{\theta}$ in an auxiliary measurement of the nuisance parameter, given that the true value is θ. We treat nuisance parameters via the frequentist paradigm, as described in Refs. [107, 108]. Constraints on nuisance parameters which alter the normalization, but not the shape, of the discriminant variable distribution for signal or background processes are represented by log-normal probability density functions (pdfs). Systematic uncertainties that affect the shape of the discriminant variable distribution, mainly the uncertainties on the lepton energy scales, are incorporated into the likelihood fit via the technique detailed in Ref. [109] and represented by nuisance parameters that are constrained by Gaussian pdfs.

Statistical uncertainties on the shape templates are accounted for by introducing additional nuisance parameters into the likelihood fit which allow for uncorrelated single-bin fluctuations of the background expectation, following the method described in Ref. [110]. In the tail of the $m_{\tau\tau}$ distribution, where the statistical uncertainties are large, a different method is used. A fit of the form $f = \exp\left(-\frac{m_{\tau\tau}}{c_0+c_1\cdot m_{\tau\tau}}\right)$ is performed for each of the major backgrounds. Depending on channel, category and background, the fit starts at $m_{\tau\tau}$ values between 150 and 325 GeV. The result of the fit replaces the nominal distribution in this region while the rest of the template, at lower masses, remains unchanged. The fit parameters c_0 and c_1 are de-correlated and represented by nuisance parameters that are allowed to vary during the likelihood fit, within the uncertainties obtained by the de-correlation procedure. Below the starting point of the fit, the bins of the nominal $m_{\tau\tau}$ distribution are used and statistical uncertainties are accounted for via nuisance parameters which allow for uncorrelated single-bin fluctuations.

We calculate exclusion limits following the modified frequentist method, $\mathrm{CL_s}$ [111, 112]. The test statistic q_μ that quantifies whether the $m_{\tau\tau}$ distribution observed in data is signal-like or background-like is given by the profile-likelihood ratio:

$$q_\mu = -2\ln\frac{\mathcal{L}\left(data|\mu,\hat{\theta}_\mu\right)}{\mathcal{L}\left(data|\hat{\mu},\hat{\theta}\right)}, \quad 0 \leq \hat{\mu} \leq \mu. \tag{4}$$

The symbol $\hat{\theta}_\mu$ in the numerator represents the nuisance parameter values that maximize the likelihood function $\mathcal{L}$ for a given value of the signal strength modifier μ that is under test. The pair $\hat{\mu}$, $\hat{\theta}$ refers to the maximum of the likelihood function within the region $\hat{\mu} \leq \mu$, which we impose in order to obtain one-sided confidence intervals on μ.

The ratio of probabilities to observe a value of the test statistic at least as large as the one observed in data, q_μ^{obs}, under the *signal+background* and under the *background-only* hypothesis,

$$\mathrm{CL_s}(\mu) = \frac{P\left(q_\mu \geq q_\mu^{obs}|\,\textit{signal+background}\right)}{P\left(q_\mu \geq q_\mu^{obs}|\,\textit{background-only}\right)}, \tag{5}$$

is used as criterion for excluding the presence of a signal of strength μ at the $1-\alpha$ confidence level (CL). To quote 95% CL upper limits on μ, we adjust the signal rate for the *signal+background* hypothesis until we reach $\mathrm{CL_s} = 0.05$.

The probabilities $P(q_\mu \geq q_\mu^{obs}|\,\textit{signal+background})$ and $P(q_\mu \geq q_\mu^{obs}|\,\textit{background-only})$ are computed by generating pseudo-data ("toys"). The toys are constructed as described in Refs. [107, 108].

The definition of the *signal+background* and of the *background-only* hypothesis is adjusted for the case of setting exclusion limits in the m_A-tan β parameter space and for the case of computing model independent upper limits on cross section times branching fraction.

In case we set limits on tan β versus m_{A}, we interpret the observed SM-like Higgs boson of mass 125 GeV as the light scalar Higgs boson h of the MSSM and modify the profile-likelihood ratio, Eq. 4, accordingly:

$$q_\mu = -2 \ln \frac{\mathcal{L}\left(data|\mu \cdot s(\hat{\theta}_\mu) + b(\hat{\theta}_\mu)\right)}{\mathcal{L}\left(data|h_{SM}(\hat{\theta}) + b(\hat{\theta})\right)}. \tag{6}$$

The symbol h_{SM} refers to the contribution expected for a Higgs boson of mass 125 GeV with SM cross section and branching fractions. The signal s in the numerator refers to the sum of all three neutral MSSM Higgs bosons, A + H + h. The sum is computed as function of m_{A} and tan β by the following procedure: The cross sections for gluon fusion and for b-quark associated production as well as the branching fraction for the decay into tau pairs are determined for each of the Higgs bosons A, H and h as described in section 3. The mass of each Higgs boson is computed using FEYNHIGGS. Tabulated values of the A, H and h masses are provided by the LHC Higgs Cross Section Working Group [41]. Shape templates for intermediate mass-points are constructed via the technique detailed in Ref. [113]. Finally, the contributions of A, H and h are normalized according to cross section times branching fraction and summed. A point in m_{A}-tan β parameter space is excluded if the $\mathrm{CL_s}$ value for the compatibility of the data with the $s + b$ versus $h_{SM} + b$ hypothesis, computed according to Eq. 5, amounts to less than 0.05. The probabilities $P(q_\mu \geq q_\mu^{obs}|\, s + b)$ and $P(q_\mu \geq q_\mu^{obs}|\, h_{SM} + b)$ are computed using toys that are generated for the $s + b$ and $h_{SM} + b$ hypothesis respectively. Note that the decision whether a point in the m_{A}-tan β parameter space is excluded or not is based on the presence or absence of evidence for further Higgs bosons in the data, beyond the resonance at 125 GeV already discovered.

In case of the model independent analysis, we search for the decays into tau pairs of a single narrow resonance ϕ of mass m_ϕ beyond the discovered resonance at 125 GeV [1]. The SM-like Higgs boson of mass 125 GeV is treated as "background" and the numerator and denominator of the profile-likelihood ratio are adjusted accordingly:

$$q_\mu = -2 \ln \frac{\mathcal{L}\left(data|\mu \cdot s(\hat{\theta}_\mu) + h_{SM}(\hat{\theta}_\mu) + b(\hat{\theta}_\mu)\right)}{\mathcal{L}\left(data|\hat{\mu} \cdot s(\hat{\theta}) + h_{SM}(\hat{\theta}) + b(\hat{\theta})\right)}, \quad 0 \leq \hat{\mu} \leq \mu. \tag{7}$$

The probabilities $P(q_\mu \geq q_\mu^{obs}|\, s + h_{SM} + b)$ and $P(q_\mu \geq q_\mu^{obs}|\, h_{SM} + b)$ are computed by means of toys that are generated for the $s + h_{SM} + b$ and $h_{SM} + b$ hypothesis respectively. Separate limits are computed for neutral MSSM Higgs boson production via gluon fusion and for the production in association with b-quarks. The rate of b-quark associated production (gluon fusion) is treated as nuisance parameter in the fit when extracting the limit on gluon fusion (in association with b-quarks).

10 Results

The event yields observed in the *b-tag* and *no-b-tag* categories of the eτ_{h}, $\mu\tau_{\mathrm{h}}$, $\tau_{\mathrm{h}}\tau_{\mathrm{h}}$, e$\mu$ and $\mu\mu$ channels are compared to the expectation for background processes and for a SM Higgs boson

[1] In the region of large m_{A} and moderate or large values of tan β in the MSSM, the heavy scalar Higgs boson H and the pseudo-scalar Higgs boson A are almost degenerate in mass and have widths that are small compared to the experimental resolution on $m_{\tau\tau}$. In this region of m_{A}-tan β parameter space the assumption of a single narrow resonance of mass m_ϕ represents a good approximation for the sum A + H.

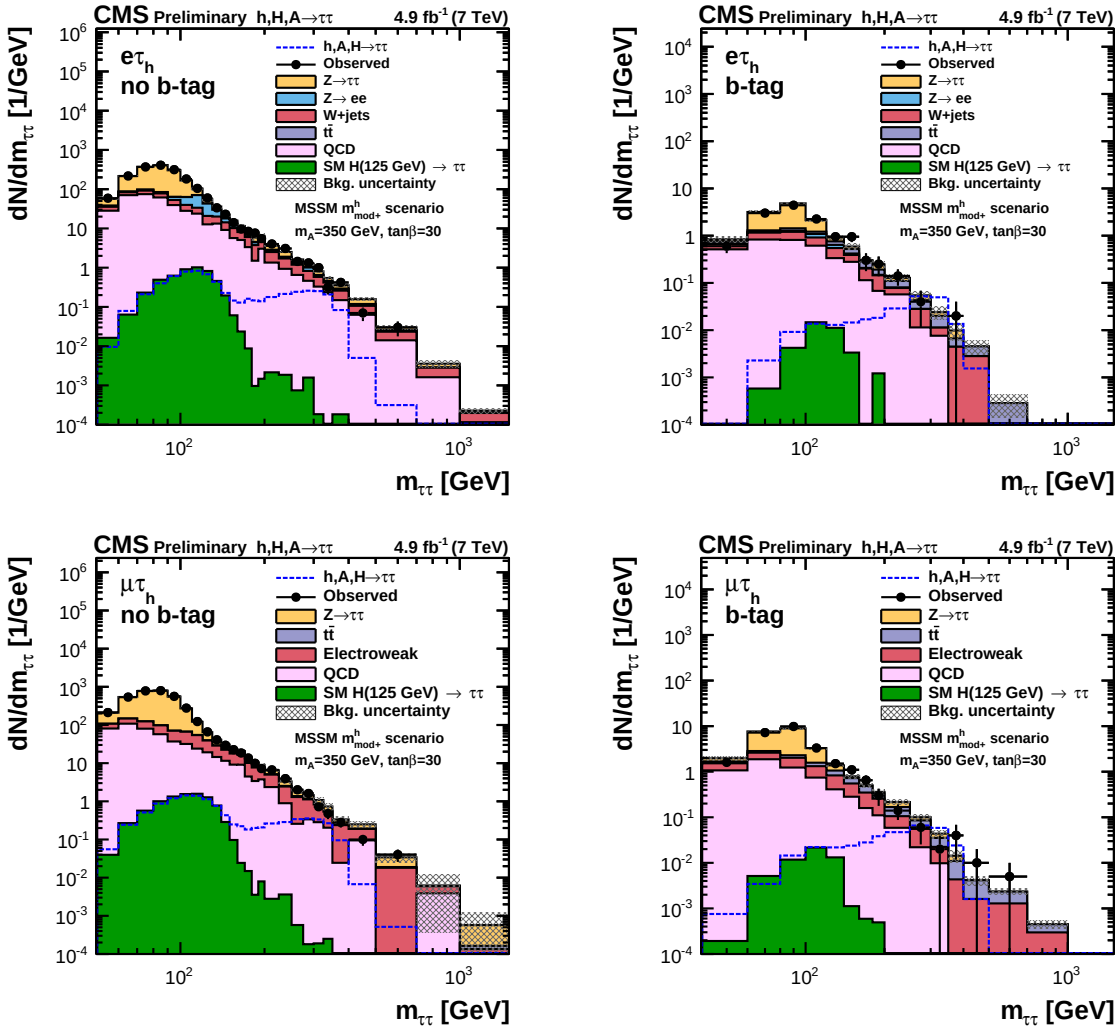

Figure 3: Distribution of tau-lepton pair invariant mass observed in the *no-b-tag* (left) and *b-tag* (right) category of the $e\tau_h$ (top) and $\mu\tau_h$ (bottom) channel in the 7 TeV data, compared to the expectation for background plus SM Higgs boson. The expectation is shown for the values of nuisance parameters obtained by the maximum likelihood fit described in section 9.

of mass 125 GeV in Tables 2 to 6. The observed tau-lepton pair invariant mass spectra are shown in Figs. 3 to 8. No clear evidence for the presence of a MSSM Higgs boson signal is observed.

We therefore proceed by setting exclusion limits in the context of different MSSM benchmark scenarios. Within each benchmark scenario, the value of the tree level parameters m_A and $\tan\beta$ are varied, while the values of other parameters, which affect the Higgs sector via radiative corrections, are fixed to certain values, chosen to cover different phenomenological characteristics. The definition of the different MSSM benchmark scenarios considered is detailed in Tab. 7.

The parameters of the m_h^{max} scenario have been chosen such that the mass of the lightest neutral MSSM Higgs boson is maximized, reaching a value of $m_h \sim 135$ GeV. This choice of parameters was motivated by yielding the most conservative m_A-$\tan\beta$ exclusion limits at LEP. The discovery of a SM-like Higgs boson of mass 125 GeV excludes a large part of the parameter space of the m_h^{max} scenario.

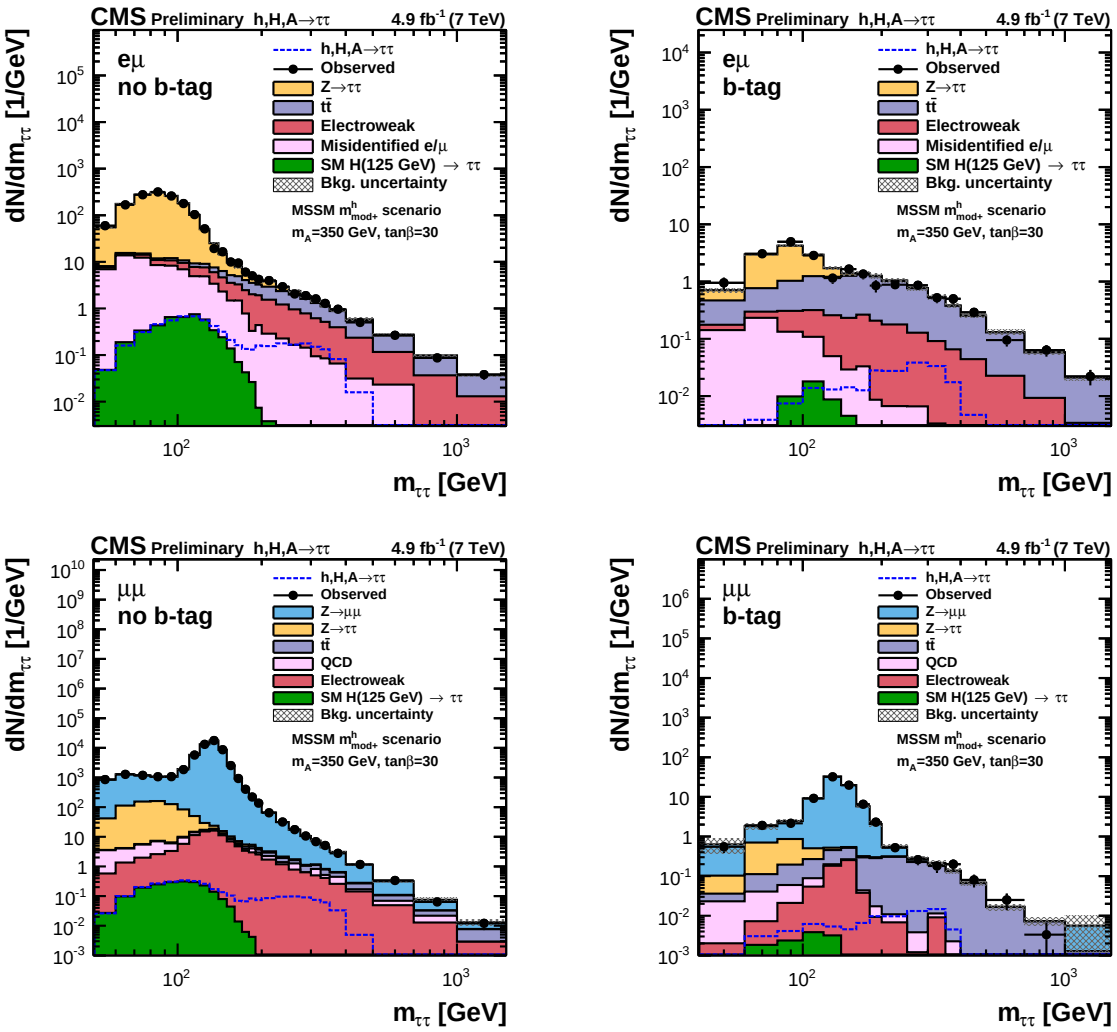

Figure 4: Distribution of tau-lepton pair invariant mass observed in the *no-b-tag* (left) and *b-tag* (right) category of the eμ (top) and $\mu\mu$ (bottom) channel in the 7 TeV data, compared to the expectation for background plus SM Higgs boson. The expectation is shown for the values of nuisance parameters obtained by the maximum likelihood fit described in section 9.

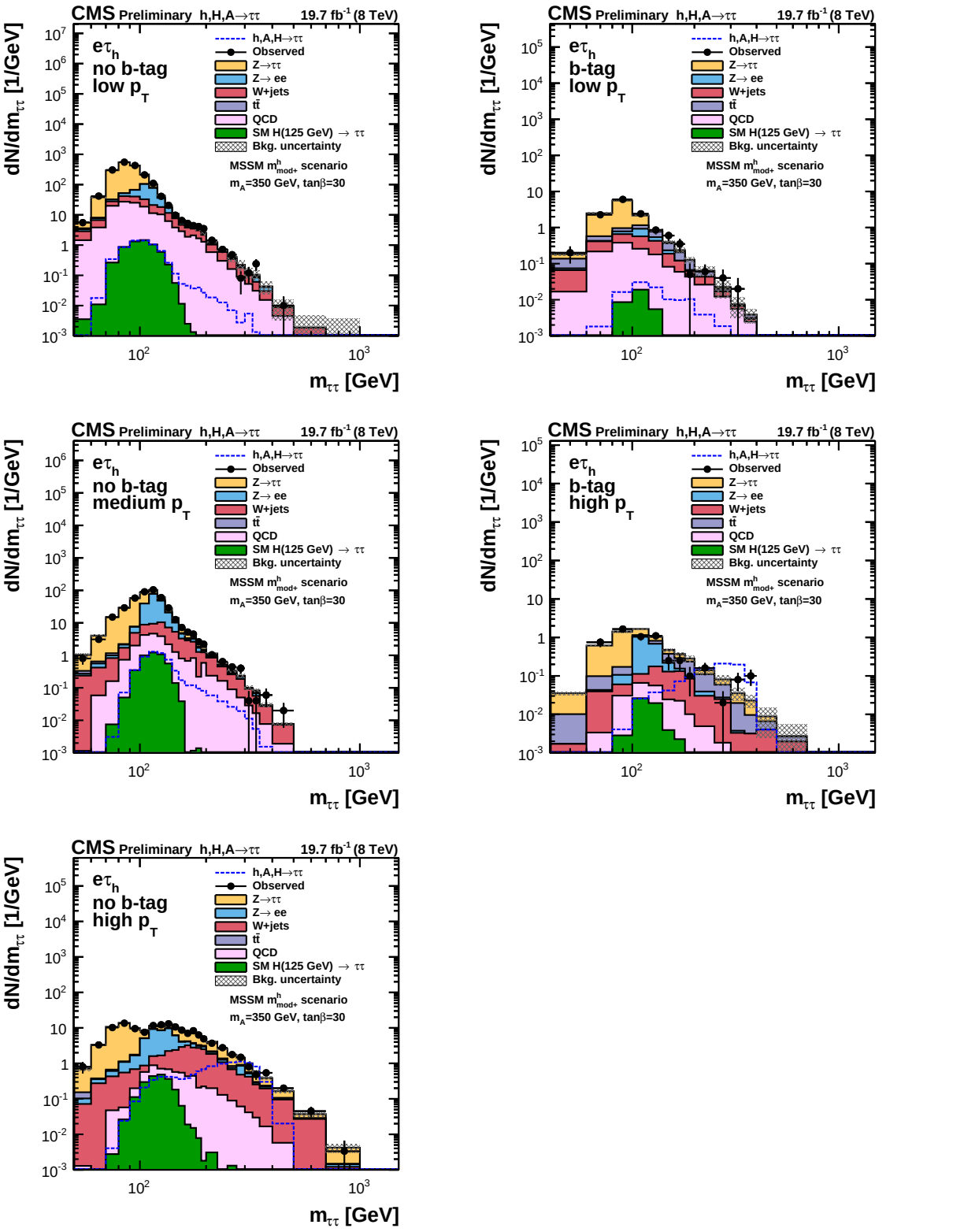

Figure 5: Distribution of tau-lepton pair invariant mass observed in the different event categories of the $e\tau_h$ channel in the 8 TeV data, compared to the expectation for background plus SM Higgs boson. The expectation is shown for the values of nuisance parameters obtained by the maximum likelihood fit described in section 9.

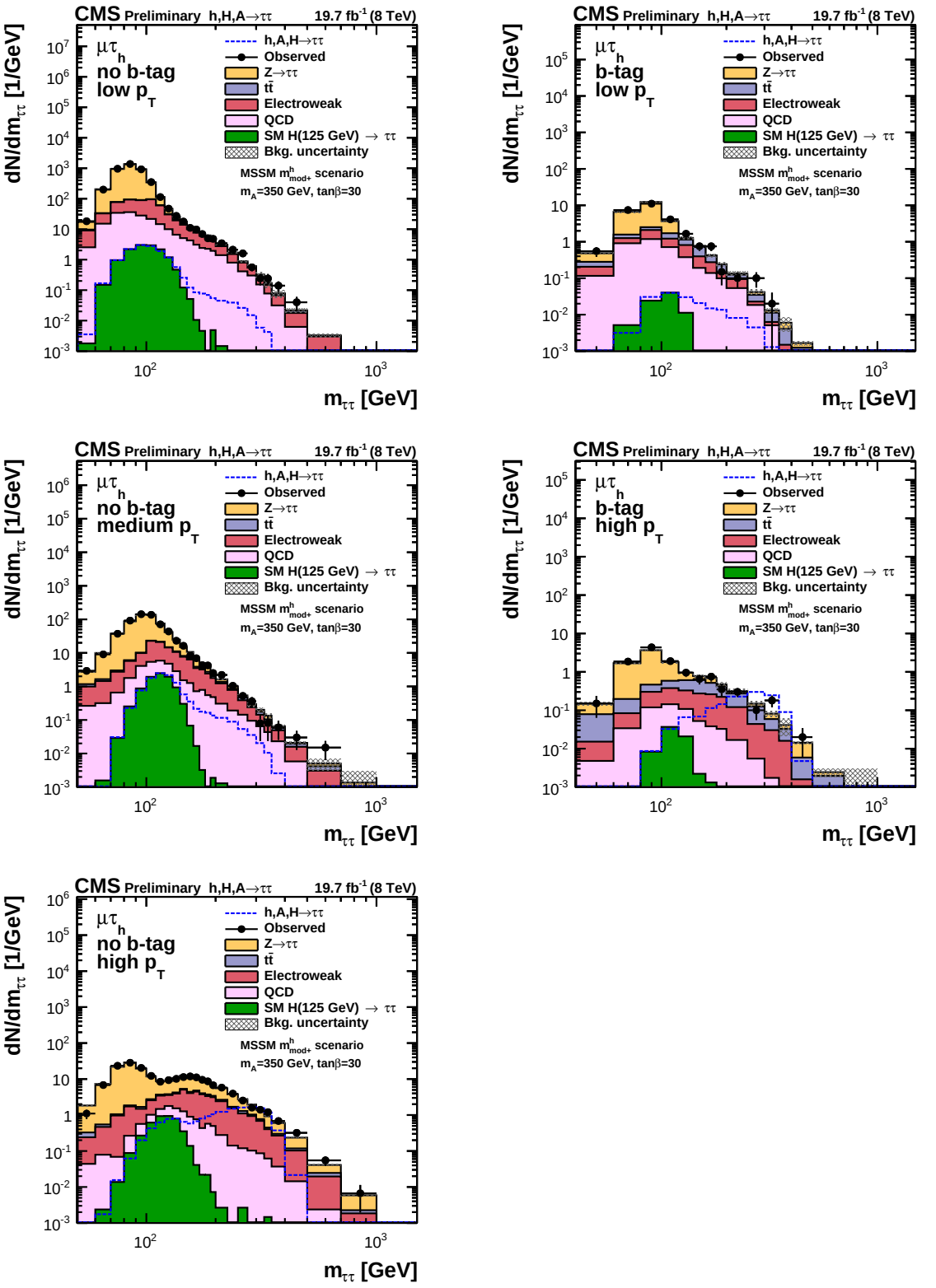

Figure 6: Distribution of tau-lepton pair invariant mass observed in the different event categories of the $\mu\tau_h$ channel in the 8 TeV data, compared to the expectation for background plus SM Higgs boson. The expectation is shown for the values of nuisance parameters obtained by the maximum likelihood fit described in section 9.

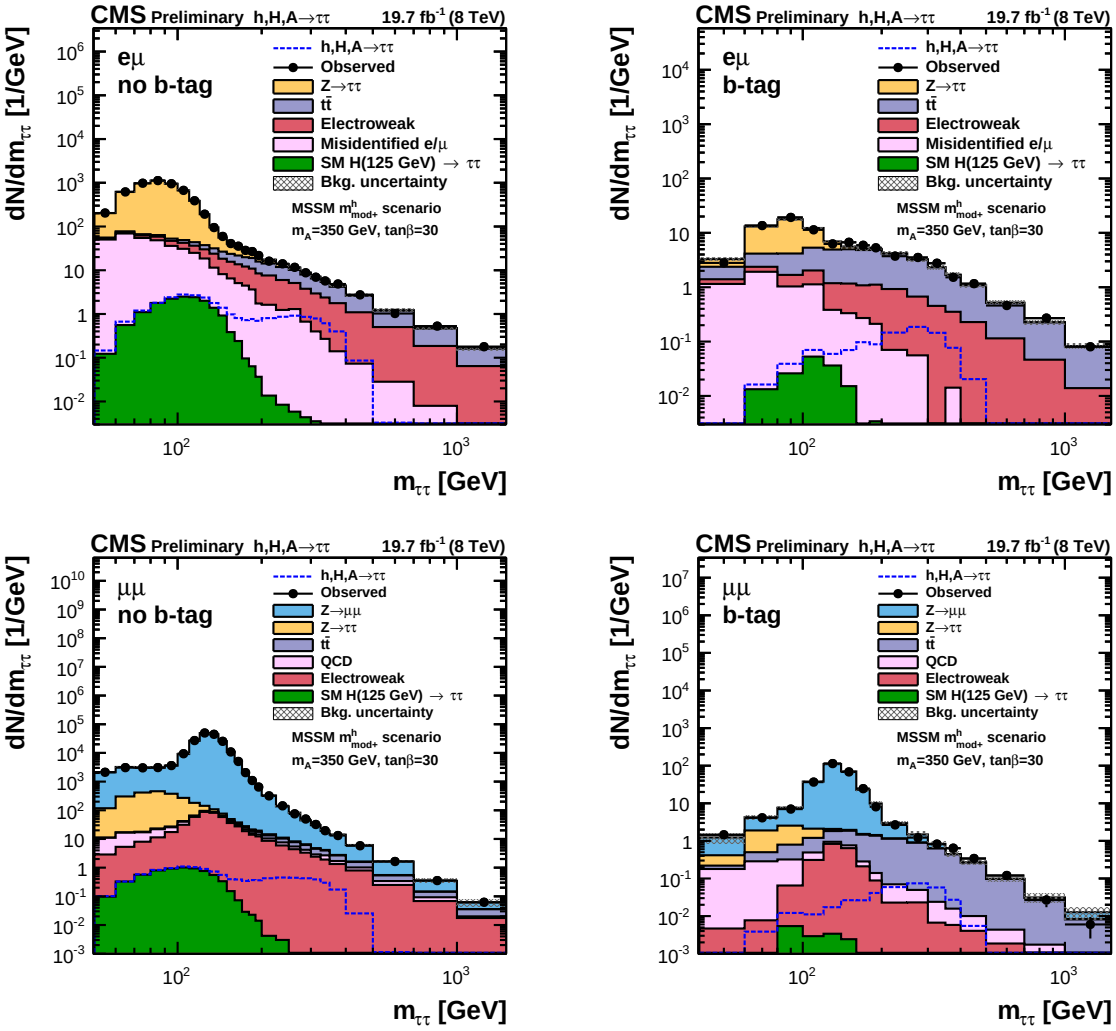

Figure 7: Distribution of tau-lepton pair invariant mass observed in the *no-b-tag* (left) and *b-tag* (right) category of the eμ (top) and $\mu\mu$ (bottom) channel in the 8 TeV data, compared to the expectation for background plus SM Higgs boson. The expectation is shown for the values of nuisance parameters obtained by the maximum likelihood fit described in section 9.

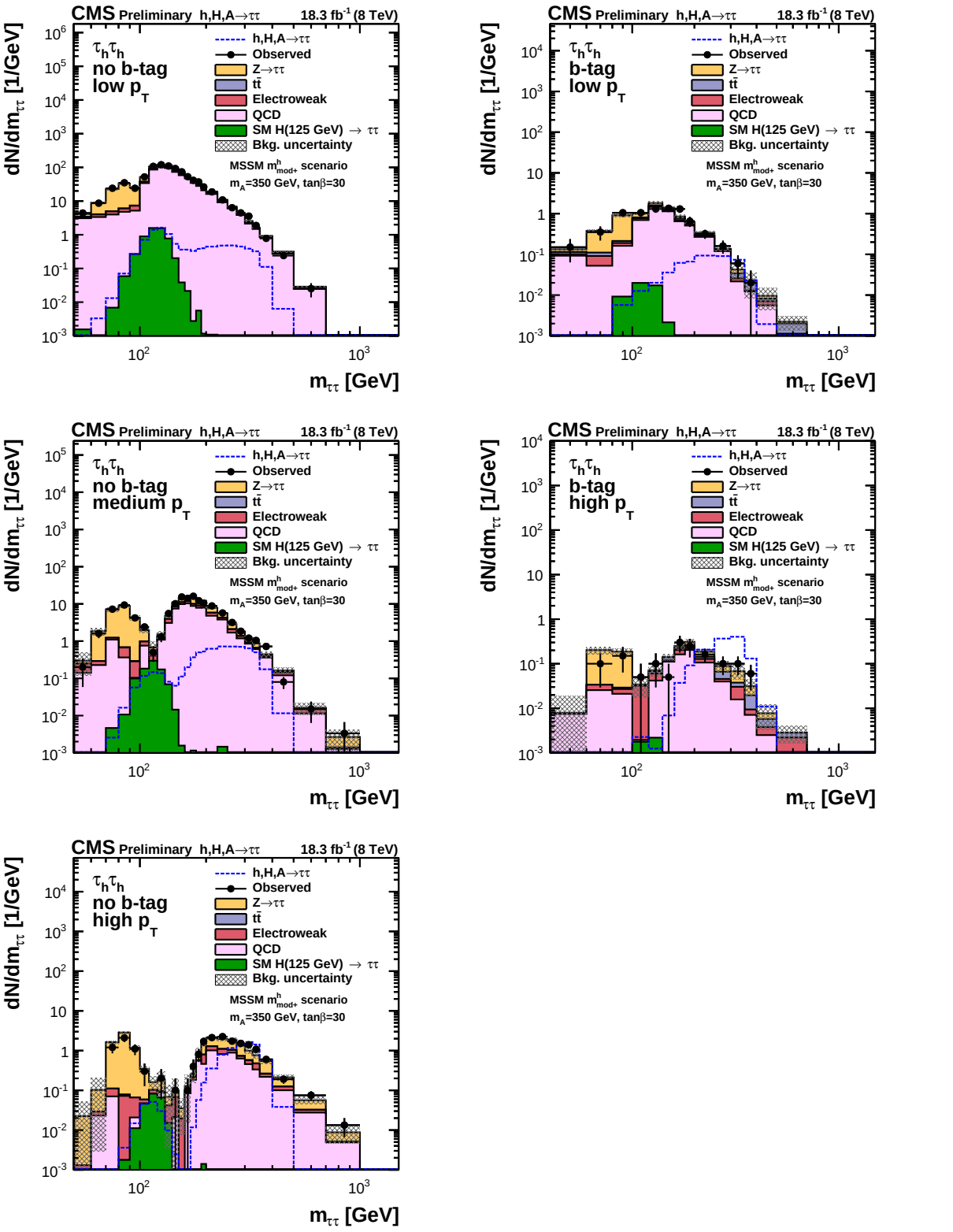

Figure 8: Distribution of tau-lepton pair invariant mass observed in the different event categories of the $\tau_h\tau_h$ channel in the 8 TeV data, compared to the expectation for background plus SM Higgs boson. The expectation is shown for the values of nuisance parameters obtained by the maximum likelihood fit described in section 9.

The $m_{\mathrm{h}}^{\mathrm{mod}+}$, $m_{\mathrm{h}}^{\mathrm{mod}-}$, *light-stop*, *light-stau* and τ-*phobic* scenarios are designed such that the light scalar h is compatible with the measured mass of the discovered SM-like Higgs boson within an uncertainty of 3 GeV. The uncertainty is dominated by the theoretical uncertainty on the prediction of m_h in supersymmetric models [58]. The present experimental uncertainty on the mass of the SM-like Higgs boson of mass 125 GeV amounts to less than 0.3 GeV [114]. The $m_{\mathrm{h}}^{\mathrm{mod}+}$ and $m_{\mathrm{h}}^{\mathrm{mod}-}$ scenarios differ from the $m_{\mathrm{h}}^{\mathrm{max}}$ scenario by the value of the stop mixing parameter. The positive (negative) sign that defines the $m_{\mathrm{h}}^{\mathrm{mod}+}$ ($m_{\mathrm{h}}^{\mathrm{mod}-}$) scenario provides the best agreement with the measured value of $(g-2)_\mu$ (rate of $b \to s\gamma$). In the *light-stop* scenario, the rate for Higgs boson production via gluon fusion is modified, while in the *light-stau* scenario the decay rate of the lightest neutral MSSM Higgs boson to photons is enhanced. The τ-*phobic* scenario has reduced Higgs couplings to down-type fermions.

The exclusion limits obtained for the $m_{\mathrm{h}}^{\mathrm{max}}$, $m_{\mathrm{h}}^{\mathrm{mod}+}$, $m_{\mathrm{h}}^{\mathrm{mod}-}$, *light-stop*, *light-stau* and τ-*phobic* scenarios are shown in Fig. 9. The region in parameter space incompatible with $m_{\mathrm{h}} = 125 \pm 3$ GeV is indicated by the hatched area in the figure. The region of low $\tan\beta$ values is excluded by the discovery of a SM-like Higgs boson of mass 125 GeV. The non-observation of a neutral MSSM Higgs boson signal decaying to tau leptons excludes a large part of the high $\tan\beta$ region plus some region in parameter space at low $\tan\beta$. We do not show limits for the *low-*m_{H} scenario, as this benchmark scenario is excluded by the searches for charged Higgs bosons [115, 116].

The model independent limits obtained on $\sigma(\mathrm{gg}\phi) \cdot \mathcal{B}(\phi \to \tau\tau)$ and $\sigma(bb\phi) \cdot \mathcal{B}(\phi \to \tau\tau)$ are shown in Fig. 10. The limits are based on the 8 TeV data only. The observed limits are in agreement with the limits expected in case no MSSM Higgs boson signal is present in the data. Tabulated values of the limits are given in the appendix. A comparison of the expected model independent limits between the previous CMS result [25] and this paper is shown in Fig. 11. For most of the scanned m_ϕ range, the expected reach on $\sigma(\mathrm{gg}\phi) \cdot \mathcal{B}(\phi \to \tau\tau)$ ($\sigma(bb\phi) \cdot \mathcal{B}(\phi \to \tau\tau)$) is increased by an amount greater than 40% (20%).

Finally, we present two-dimensional contours of the likelihood function, computed according to Eq. 3 for the case $\nu_i = \mu \cdot s_i + h_{SM_i} + b_i$, in Figs. 12 and 13. The likelihood contours preserve the full information provided by the *b-tag* and *no-b-tag* categories, as no profiling of the ggϕ and $bb\phi$ signal rates is performed. The likelihood contours exhibit no evidence for a signal beyond the discovered SM-like Higgs boson of mass 125 GeV.

11 Summary

A search for neutral MSSM Higgs bosons in the decay channel to tau pairs was presented. The search was performed in the five decay channels eτ_{h}, $\mu\tau_{\mathrm{h}}$, $\tau_{\mathrm{h}}\tau_{\mathrm{h}}$, e$\mu$ and $\mu\mu$ and in two event categories, based on the presence or absence of a b-tagged jet respectively, which provide sensitivity to the two production processes ggϕ and $bb\phi$ and enhance the overall sensitivity of the analysis.

The sensitivity of the search presented in this paper is further enhanced compared to a previous CMS analysis based on the same dataset, the results of which are superseded by this search, by using a new algorithm for the identification of hadronic tau decays and analyzing events selected in the eτ_{h}, $\mu\tau_{\mathrm{h}}$ and $\tau_{\mathrm{h}}\tau_{\mathrm{h}}$ channels in the 8 TeV data in subcategories based on hadronic tau p_T.

No evidence for a signal was found in the proton-proton collision dataset recorded by the CMS experiment during LHC run 1, corresponding to an integrated luminosity of 24.6 fb^{-1}, and corresponding exclusion limits in MSSM parameter space have been set for different MSSM

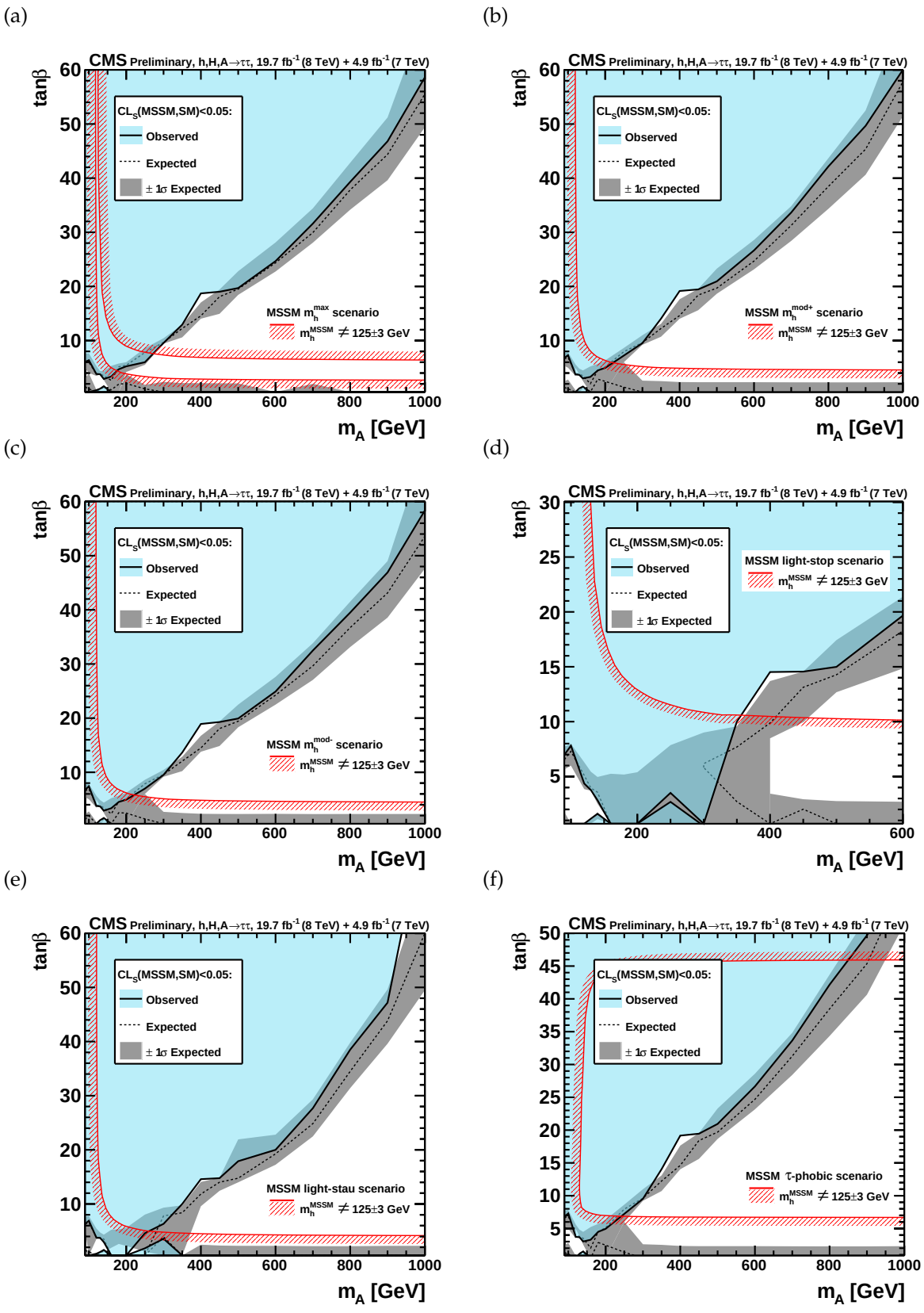

Figure 9: Region in m_{A}-tan β parameter space excluded at 95% CL in different MSSM benchmark scenarios: $m_{\mathrm{h}}^{\mathrm{max}}$ (a), $m_{\mathrm{h}}^{\mathrm{mod+}}$ (b), $m_{\mathrm{h}}^{\mathrm{mod-}}$ (c), *light-stop* (d), *light-stau* (e) and τ-*phobic* (f).

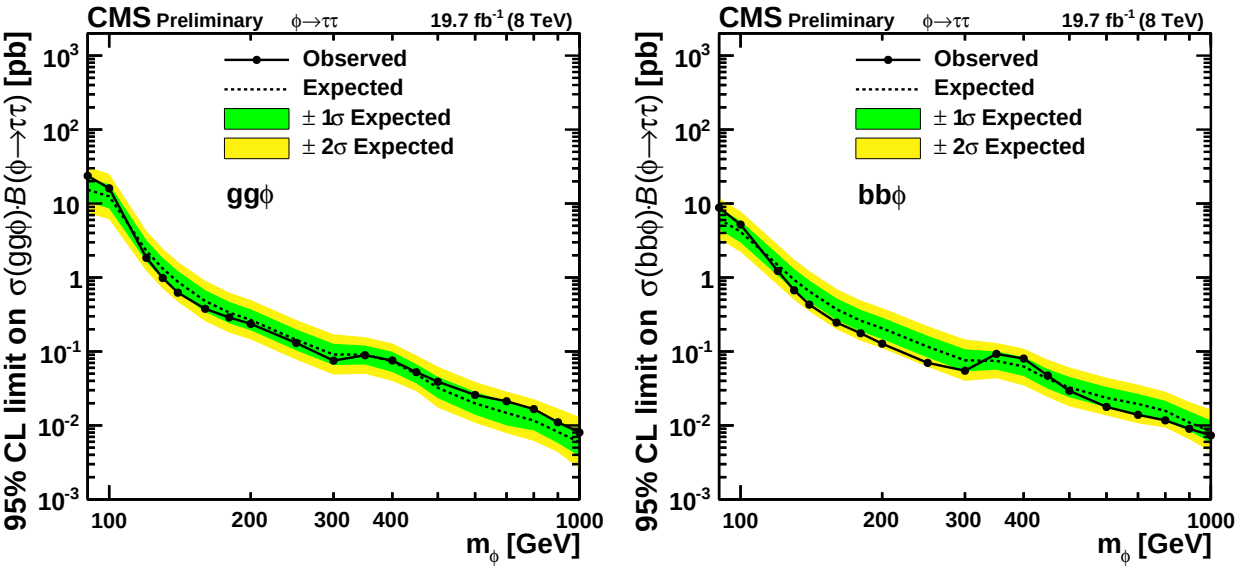

Figure 10: 95% CL upper limits on $\sigma(gg\phi) \cdot \mathcal{B}(\phi \to \tau\tau)$ (left) and $\sigma(bb\phi) \cdot \mathcal{B}(\phi \to \tau\tau)$ (right) for the production of an additional single narrow resonance ϕ of mass m_ϕ that decays into tau pairs, beyond the discovered SM-like Higgs boson of mass 125 GeV, at $\sqrt{s} = 8$ TeV center-of-mass energy.

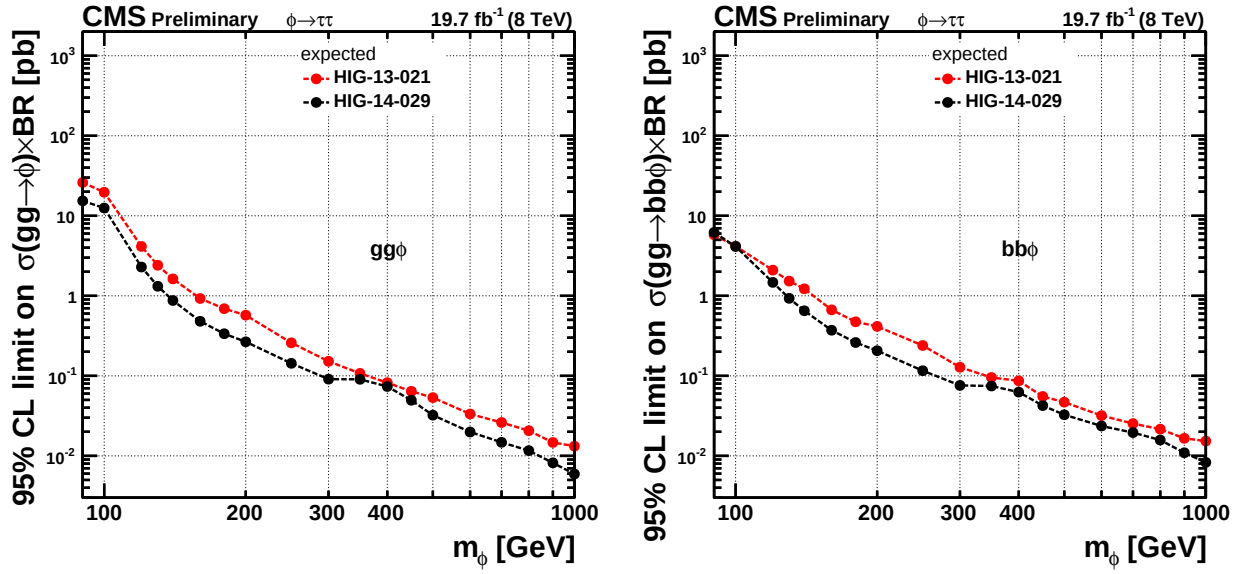

Figure 11: Comparison between the performance of the previous CMS paper (HIG-13-021) [25] and this result (HIG-14-029): expected 95% CL upper limits on $\sigma(gg\phi) \cdot \mathcal{B}(\phi \to \tau\tau)$ (left) and $\sigma(bb\phi) \cdot \mathcal{B}(\phi \to \tau\tau)$ (right) for the production of an additional single narrow resonance ϕ of mass m_ϕ that decays into tau pairs, beyond the discovered SM-like Higgs boson of mass 125 GeV, at $\sqrt{s} = 8$ TeV center-of-mass energy.

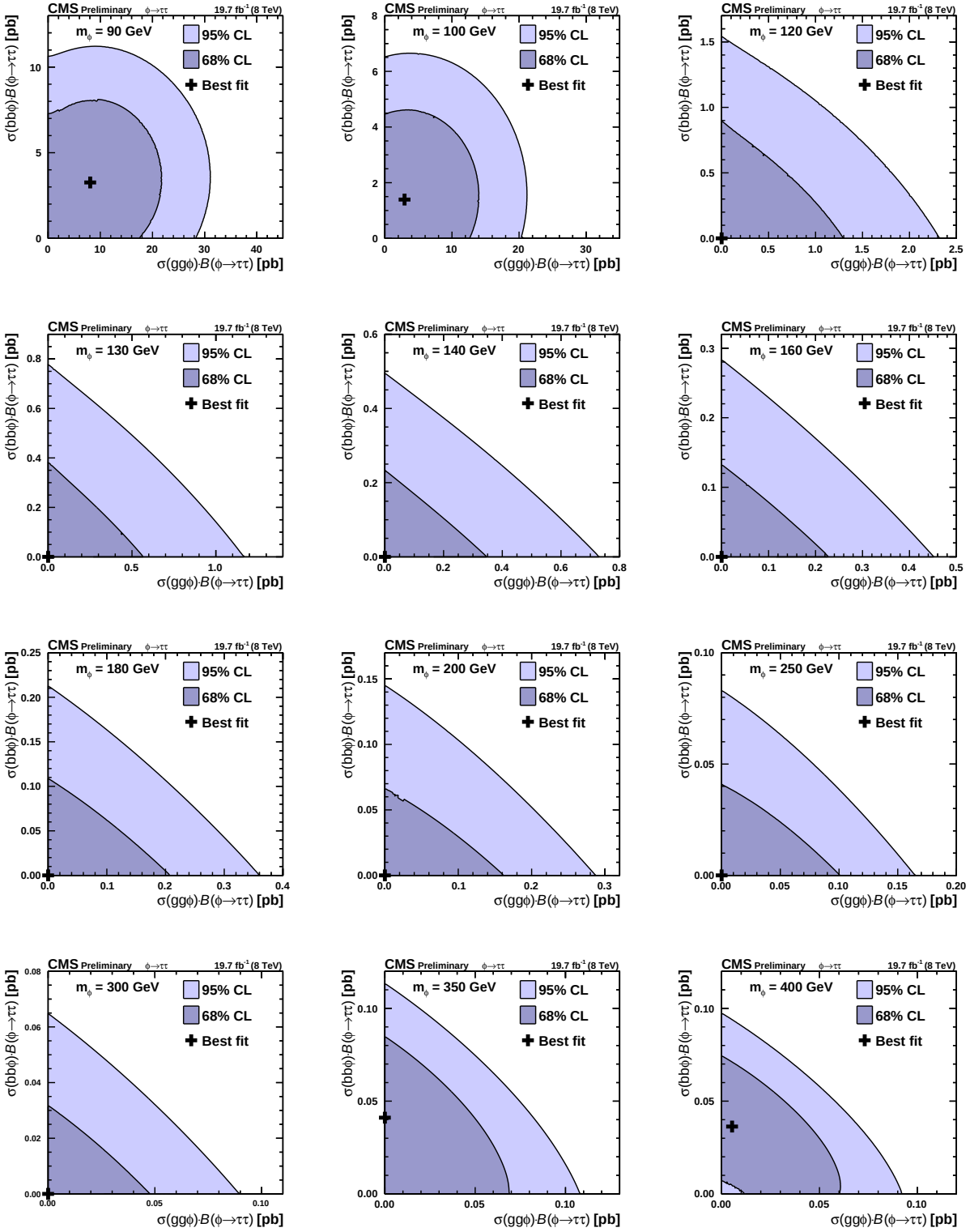

Figure 12: Contours of the likelihood function, Eq. 3, as function of $\sigma(gg\phi) \cdot \mathcal{B}(\phi \to \tau\tau)$ and $\sigma(bb\phi) \cdot \mathcal{B}(\phi \to \tau\tau)$ for the production of an additional single narrow resonance ϕ of mass m_ϕ, beyond the discovered SM-like Higgs boson of mass 125 GeV, at $\sqrt{s} = 8$ TeV center-of-mass energy, for different values of m_ϕ.

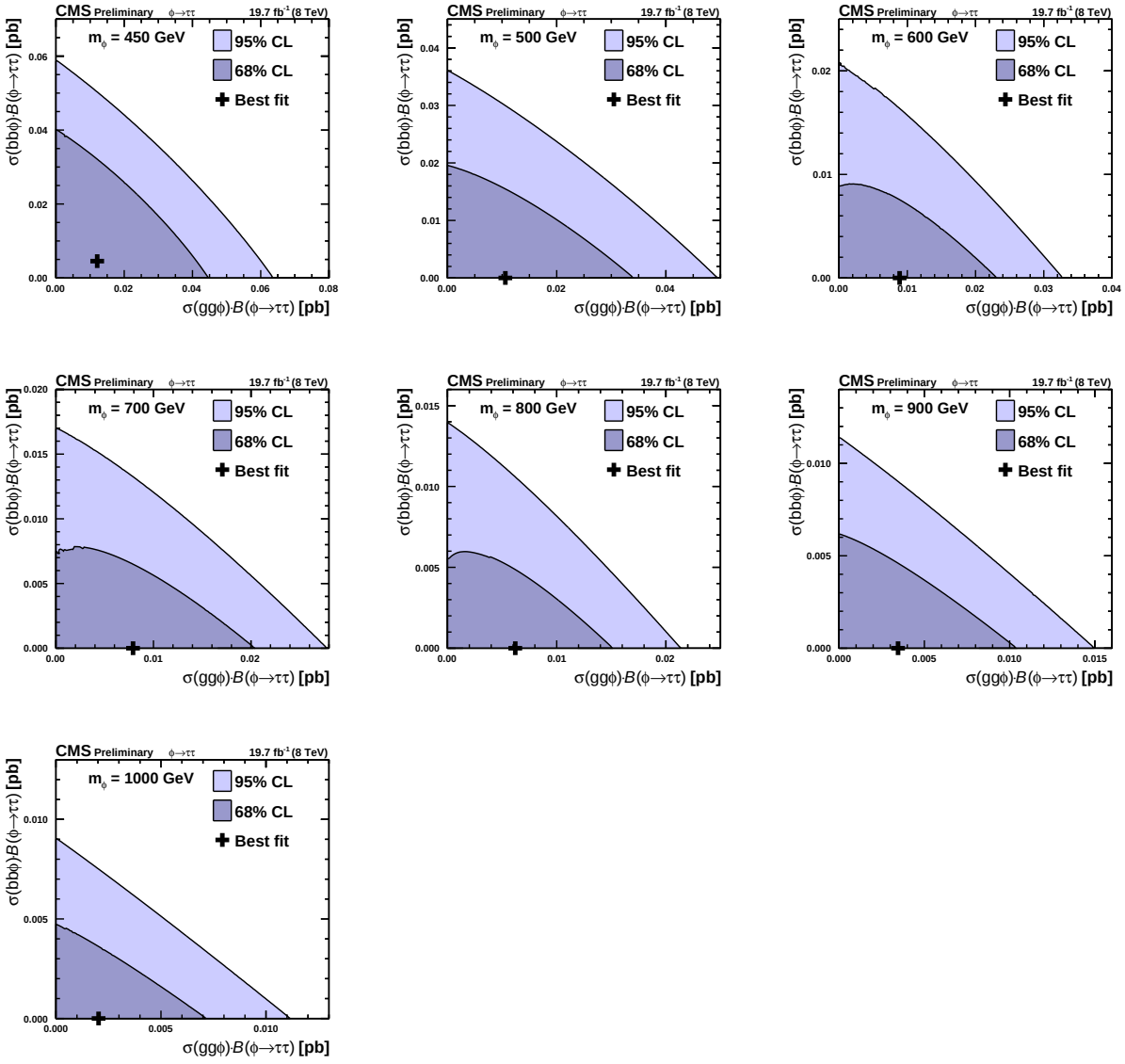

Figure 13: Contours of the likelihood function, Eq. 3, as function of $\sigma(gg\phi) \cdot \mathcal{B}(\phi \to \tau\tau)$ and $\sigma(bb\phi) \cdot \mathcal{B}(\phi \to \tau\tau)$ for the production of an additional single narrow resonance ϕ of mass m_ϕ, beyond the discovered SM-like Higgs boson of mass 125 GeV, at $\sqrt{s} = 8$ TeV center-of-mass energy, for different values of m_ϕ.

benchmark scenarios. Stringent model independent limits on cross section times branching fraction, $\sigma(gg\phi) \cdot \mathcal{B}(\phi \to \tau\tau)$ and $\sigma(bb\phi) \cdot \mathcal{B}(\phi \to \tau\tau)$, for the production of neutral MSSM Higgs bosons via gluon fusion and in association with bottom quarks have also been set.

Acknowledgements

We congratulate our colleagues in the CERN accelerator departments for the excellent performance of the LHC and thank the technical and administrative staffs at CERN and at other CMS institutes for their contributions to the success of the CMS effort. In addition, we gratefully acknowledge the computing centres and personnel of the Worldwide LHC Computing Grid for delivering so effectively the computing infrastructure essential to our analyses. Finally, we acknowledge the enduring support for the construction and operation of the LHC and the CMS detector provided by the following funding agencies: the Austrian Federal Ministry of Science, Research and Economy and the Austrian Science Fund; the Belgian Fonds de la Recherche Scientifique, and Fonds voor Wetenschappelijk Onderzoek; the Brazilian Funding Agencies (CNPq, CAPES, FAPERJ, and FAPESP); the Bulgarian Ministry of Education and Science; CERN; the Chinese Academy of Sciences, Ministry of Science and Technology, and National Natural Science Foundation of China; the Colombian Funding Agency (COLCIENCIAS); the Croatian Ministry of Science, Education and Sport, and the Croatian Science Foundation; the Research Promotion Foundation, Cyprus; the Ministry of Education and Research, Estonian Research Council via IUT23-4 and IUT23-6 and European Regional Development Fund, Estonia; the Academy of Finland, Finnish Ministry of Education and Culture, and Helsinki Institute of Physics; the Institut National de Physique Nucléaire et de Physique des Particules / CNRS, and Commissariat à l'Énergie Atomique et aux Énergies Alternatives / CEA, France; the Bundesministerium für Bildung und Forschung, Deutsche Forschungsgemeinschaft, and Helmholtz-Gemeinschaft Deutscher Forschungszentren, Germany; the General Secretariat for Research and Technology, Greece; the National Scientific Research Foundation, and National Innovation Office, Hungary; the Department of Atomic Energy and the Department of Science and Technology, India; the Institute for Studies in Theoretical Physics and Mathematics, Iran; the Science Foundation, Ireland; the Istituto Nazionale di Fisica Nucleare, Italy; the Ministry of Science, ICT and Future Planning, and National Research Foundation (NRF), Republic of Korea; the Lithuanian Academy of Sciences; the Ministry of Education, and University of Malaya (Malaysia); the Mexican Funding Agencies (CINVESTAV, CONACYT, SEP, and UASLP-FAI); the Ministry of Business, Innovation and Employment, New Zealand; the Pakistan Atomic Energy Commission; the Ministry of Science and Higher Education and the National Science Centre, Poland; the Fundação para a Ciência e a Tecnologia, Portugal; JINR, Dubna; the Ministry of Education and Science of the Russian Federation, the Federal Agency of Atomic Energy of the Russian Federation, Russian Academy of Sciences, and the Russian Foundation for Basic Research; the Ministry of Education, Science and Technological Development of Serbia; the Secretaría de Estado de Investigación, Desarrollo e Innovación and Programa Consolider-Ingenio 2010, Spain; the Swiss Funding Agencies (ETH Board, ETH Zurich, PSI, SNF, UniZH, Canton Zurich, and SER); the Ministry of Science and Technology, Taipei; the Thailand Center of Excellence in Physics, the Institute for the Promotion of Teaching Science and Technology of Thailand, Special Task Force for Activating Research and the National Science and Technology Development Agency of Thailand; the Scientific and Technical Research Council of Turkey, and Turkish Atomic Energy Authority; the National Academy of Sciences of Ukraine, and State Fund for Fundamental Researches, Ukraine; the Science and Technology Facilities Council, UK; the US Department of Energy, and the US National Science Foundation.

Individuals have received support from the Marie-Curie programme and the European Re-

search Council and EPLANET (European Union); the Leventis Foundation; the A. P. Sloan Foundation; the Alexander von Humboldt Foundation; the Belgian Federal Science Policy Office; the Fonds pour la Formation à la Recherche dans l'Industrie et dans l'Agriculture (FRIA-Belgium); the Agentschap voor Innovatie door Wetenschap en Technologie (IWT-Belgium); the Ministry of Education, Youth and Sports (MEYS) of the Czech Republic; the Council of Science and Industrial Research, India; the HOMING PLUS programme of the Foundation for Polish Science, cofinanced from European Union, Regional Development Fund; the Compagnia di San Paolo (Torino); the Consorzio per la Fisica (Trieste); MIUR project 20108T4XTM (Italy); the Thalis and Aristeia programmes cofinanced by EU-ESF and the Greek NSRF; the National Priorities Research Program by Qatar National Research Fund; and Rachadapisek Sompot Fund for Postdoctoral Fellowship, Chulalongkorn University (Thailand).

References

[1] S. L. Glashow, "Partial Symmetries of Weak Interactions", *Nucl. Phys.* **22** (1961) 579, doi:10.1016/0029-5582(61)90469-2.

[2] S. Weinberg, "A Model of Leptons", *Phys. Rev. Lett.* **19** (1967) 1264, doi:10.1103/PhysRevLett.19.1264.

[3] A. Salam, "Weak and electromagnetic interactions", in *Elementary particle physics: relativistic groups and analyticity*, N. Svartholm, ed., p. 367. Almqvist & Wiskell, Stockholm, 1968. Proceedings of the eighth Nobel symposium.

[4] F. Englert and R. Brout, "Broken Symmetry and the Mass of Gauge Vector Mesons", *Phys. Rev. Lett.* **13** (1964) 321, doi:10.1103/PhysRevLett.13.321.

[5] P. W. Higgs, "Broken symmetries, massless particles and gauge fields", *Phys. Lett.* **12** (1964) 132, doi:10.1016/0031-9163(64)91136-9.

[6] P. W. Higgs, "Broken Symmetries and the Masses of Gauge Bosons", *Phys. Rev. Lett.* **13** (1964) 508, doi:10.1103/PhysRevLett.13.508.

[7] G. S. Guralnik, C. R. Hagen, and T. W. B. Kibble, "Global Conservation Laws and Massless Particles", *Phys. Rev. Lett.* **13** (1964) 585, doi:10.1103/PhysRevLett.13.585.

[8] P. W. Higgs, "Spontaneous Symmetry Breakdown without Massless Bosons", *Phys. Rev.* **145** (1966) 1156, doi:10.1103/PhysRev.145.1156.

[9] T. W. B. Kibble, "Symmetry breaking in non-Abelian gauge theories", *Phys. Rev.* **155** (1967) 1554, doi:10.1103/PhysRev.155.1554.

[10] CMS Collaboration, "Observation of a new boson at a mass of 125 GeV with the CMS experiment at the LHC", *Phys.Lett.* **B716** (2012) 30–61, doi:10.1016/j.physletb.2012.08.021, arXiv:1207.7235.

[11] ATLAS Collaboration, "Observation of a new particle in the search for the Standard Model Higgs boson with the ATLAS detector at the LHC", *Phys.Lett.* **B716** (2012) 1–29, doi:10.1016/j.physletb.2012.08.020, arXiv:1207.7214.

[12] CMS Collaboration, "Constraints on anomalous HVV interactions using $H \to 4\ell$ decays", CMS Physics Analysis Summary CMS-PAS-HIG-14-014, 2014.

[13] CMS Collaboration Collaboration, "Search for invisible decays of Higgs bosons in the vector boson fusion and associated ZH production modes", *Eur.Phys.J.* **C74** (2014), no. 8, 2980, doi:10.1140/epjc/s10052-014-2980-6, arXiv:1404.1344.

[14] CMS Collaboration Collaboration, "Constraints on the Higgs boson width from off-shell production and decay to Z-boson pairs", *Phys.Lett.* **B736** (2014) 64, doi:10.1016/j.physletb.2014.06.077, arXiv:1405.3455.

[15] CMS Collaboration, "Precise determination of the mass of the Higgs boson and tests of compatibility of its couplings with the standard model predictions using proton collisions at 7 and 8 TeV", *Eur.Phys.J.* **C75** (2015), no. 5, 212, doi:10.1140/epjc/s10052-015-3351-7, arXiv:1412.8662.

[16] Y. A. Golfand and E. P. Likhtman, "Extension of the Algebra of Poincare Group Generators and Violation of p Invariance", *JETP Lett.* **13** (1971) 323.

[17] J. Wess and B. Zumino, "Supergauge transformations in four dimensions", *Nucl. Phys. B* **70** (1974) 39, doi:10.1016/0550-3213(74)90355-1.

[18] J. R. Ellis, S. Kelley, and D. V. Nanopoulos, "Probing the desert using gauge coupling unification", *Phys.Lett.* **B260** (1991) 131–137, doi:10.1016/0370-2693(91)90980-5.

[19] P. Langacker and M.-x. Luo, "Implications of precision electroweak experiments for M_t, ρ_0, $\sin^2\theta_W$ and grand unification", *Phys.Rev.* **D44** (1991) 817–822, doi:10.1103/PhysRevD.44.817.

[20] G. Jungman, M. Kamionkowski, and K. Griest, "Supersymmetric dark matter", *Phys.Rept.* **267** (1996) 195–373, doi:10.1016/0370-1573(95)00058-5, arXiv:hep-ph/9506380.

[21] P. Fayet, "Supergauge invariant extension of the Higgs mechanism and a model for the electron and its neutrino", *Nucl. Phys. B* **90** (1975) 104, doi:10.1016/0550-3213(75)90636-7.

[22] P. Fayet, "Spontaneously broken supersymmetric theories of weak, electromagnetic and strong interactions", *Phys. Lett. B* **69** (1977) 489, doi:10.1016/0370-2693(77)90852-8.

[23] CMS Collaboration, "Search for Neutral MSSM Higgs Bosons Decaying to Tau Pairs in pp Collisions at $\sqrt{s} = 7$ TeV", *Phys. Rev. Lett.* **106** (2011) 231801, doi:10.1103/PhysRevLett.106.231801, arXiv:1104.1619.

[24] CMS Collaboration, "Search for a Higgs boson decaying into a b-quark pair and produced in association with b quarks in proton-proton collisions at 7 TeV", *Phys. Lett. B* **722** (2013) 207, doi:10.1016/j.physletb.2013.04.017, arXiv:1302.2892.

[25] CMS Collaboration, "Search for neutral MSSM Higgs bosons decaying to a pair of tau leptons in pp collisions", *JHEP* **1410** (2014) 160, doi:10.1007/JHEP10(2014)160, arXiv:1408.3316.

[26] ATLAS Collaboration, "Search for neutral MSSM Higgs bosons decaying to $\tau^+\tau^-$ pairs in proton-proton collisions at $\sqrt{s} = 7$ TeV with the ATLAS detector", *Phys. Lett. B* **705** (2011) 174, doi:10.1016/j.physletb.2011.10.001, arXiv:1107.5003.

[27] CDF Collaboration, "Search for Higgs bosons predicted in two-Higgs-doublet models via decays to tau lepton pairs in 1.96-TeV p anti-p collisions", *Phys. Rev. Lett.* **103** (2009) 201801, doi:10.1103/PhysRevLett.103.201801, arXiv:0906.1014.

[28] D0 Collaboration, "Search for neutral Higgs bosons in the multi-b-jet topology in 5.2 fb^{-1} of $p\bar{p}$ collisions at $\sqrt{s} = 1.96$ TeV", *Phys. Lett. B* **698** (2011) 97, doi:10.1016/j.physletb.2011.02.062, arXiv:1011.1931.

[29] D0 Collaboration, "Search for Higgs bosons decaying to $\tau\tau$ pairs in $p\bar{p}$ collisions at $\sqrt{s} = 1.96$ TeV", *Phys. Lett. B* **707** (2012) 323, doi:10.1016/j.physletb.2011.12.050, arXiv:1106.4555.

[30] CDF Collaboration, "Search for Higgs bosons produced in association with b quarks", *Phys. Rev. D* **85** (2012) 032005, doi:10.1103/PhysRevD.85.032005, arXiv:1106.4782.

[31] ALEPH, DELPHI, L3, OPAL Collaborations, and the LEP Working Group for Higgs Boson Searches, S. Schael et al., "Search for neutral MSSM Higgs bosons at LEP", *Eur. Phys. J. C* **47** (2006) 547, doi:10.1140/epjc/s2006-02569-7, arXiv:hep-ex/0602042.

[32] M. S. Carena, S. Heinemeyer, C. Wagner, and G. Weiglein, "Suggestions for benchmark scenarios for MSSM Higgs boson searches at hadron colliders", *Eur.Phys.J.* **C26** (2003) 601–607, doi:10.1140/epjc/s2002-01084-3, arXiv:hep-ph/0202167.

[33] M. Carena et al., "MSSM Higgs Boson Searches at the LHC: Benchmark Scenarios after the Discovery of a Higgs-like Particle", *Eur.Phys.J.* **C73** (2013) 2552, doi:10.1140/epjc/s10052-013-2552-1, arXiv:1302.7033.

[34] CMS Collaboration, "Tau ID Performance Plots", CMS Physics CMS-DP-2014-015, 2014.

[35] CMS Collaboration, "Tau reconstruction and identification in CMS during LHC run 1", in preparation.

[36] A. Hoecker et al., "TMVA: Toolkit for Multivariate Data Analysis", *PoS* **ACAT** (2007) 040, arXiv:physics/0703039.

[37] CMS Collaboration Collaboration, "Evidence for the 125 GeV Higgs boson decaying to a pair of τ leptons", *JHEP* **1405** (2014) 104, doi:10.1007/JHEP05(2014)104, arXiv:1401.5041.

[38] CMS Collaboration, "The CMS experiment at the CERN LHC", *JINST* **3** (2008) S08004, doi:10.1088/1748-0221/3/08/S08004.

[39] T. Sjostrand, S. Mrenna, and P. Z. Skands, "PYTHIA 6.4 Physics and Manual", *JHEP* **0605** (2006) 026, doi:10.1088/1126-6708/2006/05/026, arXiv:hep-ph/0603175.

[40] S. Frixione, P. Nason, and C. Oleari, "Matching NLO QCD computations with Parton Shower simulations: the POWHEG method", *JHEP* **0711** (2007) 070, arXiv:0709.2092.

[41] LHC Higgs Cross Section Working Group, "Handbook of LHC Higgs Cross Sections: 1. Inclusive Observables", CERN Report CERN-2011-002, 2011. doi:10.5170/CERN-2011-002, arXiv:1101.0593.

[42] R. V. Harlander, S. Liebler, and H. Mantler, "SusHi: A program for the calculation of Higgs production in gluon fusion and bottom-quark annihilation in the Standard Model and the MSSM", *Comput. Phys. Commun.* **184** (2013) 1605, doi:10.1016/j.cpc.2013.02.006, arXiv:1212.3249.

[43] R. V. Harlander and M. Steinhauser, "Supersymmetric Higgs production in gluon fusion at next-to-leading order", *JHEP* **09** (2004) 066, doi:10.1088/1126-6708/2004/09/066, arXiv:hep-ph/0409010.

[44] R. V. Harlander and P. Kant, "Higgs production and decay: Analytic results at next-to-leading order QCD", *JHEP* **12** (2005) 015, doi:10.1088/1126-6708/2005/12/015, arXiv:hep-ph/0509189.

[45] G. Degrassi and P. Slavich, "NLO QCD bottom corrections to Higgs boson production in the MSSM", *JHEP* **11** (2010) 044, doi:10.1007/JHEP11(2010)044, arXiv:1007.3465.

[46] G. Degrassi, S. Di Vita, and P. Slavich, "NLO QCD corrections to pseudoscalar Higgs production in the MSSM", *JHEP* **08** (2011) 128, doi:10.1007/JHEP08(2011)128, arXiv:1107.0914.

[47] G. Degrassi, S. Di Vita, and P. Slavich, "On the NLO QCD corrections to the production of the heaviest neutral Higgs scalar in the MSSM", *Eur. Phys. J. C* **72** (2012) 2032, doi:10.1140/epjc/s10052-012-2032-z, arXiv:1204.1016.

[48] U. Aglietti, R. Bonciani, G. Degrassi, and A. Vicini, "Two loop light fermion contribution to Higgs production and decays", *Phys. Lett. B* **595** (2004) 432, doi:10.1016/j.physletb.2004.06.063, arXiv:hep-ph/0404071.

[49] R. Bonciani, G. Degrassi, and A. Vicini, "On the generalized harmonic polylogarithms of one complex variable", *Comput. Phys. Commun.* **182** (2011) 1253, doi:10.1016/j.cpc.2011.02.011, arXiv:1007.1891.

[50] M. Spira, A. Djouadi, D. Graudenz, and P. M. Zerwas, "Higgs boson production at the LHC", *Nucl. Phys. B* **453** (1995) 17, doi:10.1016/0550-3213(95)00379-7, arXiv:hep-ph/9504378.

[51] M. Spira, "HIGLU: A program for the calculation of the total Higgs production cross-section at hadron colliders via gluon fusion including QCD corrections", DESY Report DESY-T-95-05, 1995. arXiv:hep-ph/9510347.

[52] S. Dittmaier, M. Krämer, and M. Spira, "Higgs radiation off bottom quarks at the Tevatron and the CERN LHC", *Phys. Rev. D* **70** (2004) 074010, doi:10.1103/PhysRevD.70.074010, arXiv:hep-ph/0309204.

[53] S. Dawson, C. B. Jackson, L. Reina, and D. Wackeroth, "Exclusive Higgs boson production with bottom quarks at hadron colliders", *Phys. Rev. D* **69** (2004) 074027, doi:10.1103/PhysRevD.69.074027, arXiv:hep-ph/0311067.

[54] R. V. Harlander and W. B. Kilgore, "Higgs boson production in bottom quark fusion at next-to-next-to leading order", *Phys. Rev. D* **68** (2003) 013001, doi:10.1103/PhysRevD.68.013001, arXiv:hep-ph/0304035.

[55] R. V. Harlander, M. Krämer, and M. Schumacher, "Bottom-quark associated Higgs-boson production: reconciling the four- and five-flavour scheme approach", Technical Report CERN-PH-TH-2011-134, FR-PHENO-2011-009, TTK-11-17, WUB-11-04, 2011. arXiv:1112.3478.

[56] S. Heinemeyer, W. Hollik, and G. Weiglein, "FeynHiggs: A Program for the calculation of the masses of the neutral CP even Higgs bosons in the MSSM", *Comput. Phys. Commun.* **124** (2000) 76, doi:10.1016/S0010-4655(99)00364-1, arXiv:hep-ph/9812320.

[57] S. Heinemeyer, W. Hollik, and G. Weiglein, "The Masses of the neutral $\mathcal{CP}$-even Higgs bosons in the MSSM: Accurate analysis at the two-loop level", *Eur. Phys. J. C* **9** (1999) 343, doi:10.1007/s100529900006, arXiv:hep-ph/9812472.

[58] G. Degrassi et al., "Towards high precision predictions for the MSSM Higgs sector", *Eur. Phys. J. C* **28** (2003) 133, doi:10.1140/epjc/s2003-01152-2, arXiv:hep-ph/0212020.

[59] M. Frank et al., "The Higgs boson masses and mixings of the complex MSSM in the Feynman-diagrammatic approach", *JHEP* **02** (2007) 047, doi:10.1088/1126-6708/2007/02/047, arXiv:hep-ph/0611326.

[60] M. Spira, "QCD effects in Higgs physics", *Fortsch. Phys.* **46** (1998) 203, doi:10.1002/(SICI)1521-3978(199804)46:3<203::AID-PROP203>3.0.CO;2-4, arXiv:hep-ph/9705337.

[61] A. Djouadi, J. Kalinowski, and M. Spira, "HDECAY: A Program for Higgs boson decays in the standard model and its supersymmetric extension", *Comput. Phys. Commun.* **108** (1998) 56, doi:10.1016/S0010-4655(97)00123-9, arXiv:hep-ph/9704448.

[62] A. Djouadi, M. M. Mühlleitner, and M. Spira, "Decays of supersymmetric particles: The Program SUSY-HIT (SUspect-SdecaY-Hdecay-InTerface)", *Acta Phys. Polon. B* **38** (2007) 635, arXiv:hep-ph/0609292.

[63] LHC Higgs Cross Section Working Group, "Handbook of LHC Higgs Cross Sections: 3. Higgs Properties", CERN Report CERN-2013-004, 2013. doi:10.5170/CERN-2013-004, arXiv:1307.1347.

[64] J. Alwall et al., "The automated computation of tree-level and next-to-leading order differential cross sections, and their matching to parton shower simulations", *JHEP* **07** (2014) 079, doi:10.1007/JHEP07(2014)079, arXiv:1405.0301.

[65] K. Melnikov and F. Petriello, "Electroweak gauge boson production at hadron colliders through O(alpha(s)**2)", *Phys.Rev.* **D74** (2006) 114017, doi:10.1103/PhysRevD.74.114017, arXiv:hep-ph/0609070.

[66] CMS Collaboration Collaboration, "Measurement of the $t\bar{t}$ production cross section in the dilepton channel in pp collisions at $\sqrt{s}$ = 8 TeV", *JHEP* **1402** (2014) 024, doi:10.1007/JHEP02(2014)024, arXiv:1312.7582.

[67] CMS Collaboration Collaboration, "Measurement of differential top-quark pair production cross sections in pp colisions at $\sqrt{s} = 7$ TeV", *Eur.Phys.J.* **C73** (2013) 2339, doi:10.1140/epjc/s10052-013-2339-4, arXiv:1211.2220.

[68] CMS Collaboration, "Measurement of differential top-quark pair production cross sections in the lepton+jets channel in pp collisions at $\sqrt{s} = 8$ TeV", *CMS PAS* **TOP-12-027** (2012).

[69] CMS Collaboration, "Measurement of the differential top-quark pair production cross section in the dilepton channel in pp collisions at $\sqrt{s} = 8$ TeV", *CMS PAS* **TOP-12-028** (2012).

[70] J. M. Campbell, R. K. Ellis, and C. Williams, "Vector boson pair production at the LHC", *JHEP* **1107** (2011) 018, doi:10.1007/JHEP07(2011)018, arXiv:1105.0020.

[71] CMS Collaboration Collaboration, "Measurement of the Underlying Event Activity at the LHC with $\sqrt{s} = 7$ TeV and Comparison with $\sqrt{s} = 0.9$ TeV", *JHEP* **1109** (2011) 109, doi:10.1007/JHEP09(2011)109, arXiv:1107.0330.

[72] S. Jadach, Z. Was, R. Decker, and J. H. Kuhn, "The Tau Decay Library Tauola: Version 2.4", *Comput. Phys. Commun.* **76** (1993) 361.

[73] J. Pumplin et al., "New generation of parton distributions with uncertainties from global QCD analysis", *JHEP* **0207** (2002) 012, doi:10.1088/1126-6708/2002/07/012, arXiv:hep-ph/0201195.

[74] GEANT4 Collaboration, "GEANT4: A Simulation toolkit", *Nucl.Instrum.Meth.* **A506** (2003) 250–303, doi:10.1016/S0168-9002(03)01368-8.

[75] CMS Collaboration, "Particle–Flow Event Reconstruction in CMS and Performance for Jets, Taus, and $E_{\mathrm{T}}^{\mathrm{miss}}$", CMS Physics Analysis Summary CMS-PAS-PFT-09-001, 2009.

[76] CMS Collaboration, "Commissioning of the Particle-flow Event Reconstruction with the first LHC collisions recorded in the CMS detector", CMS Physics Analysis Summary CMS-PAS-PFT-10-001, 2010.

[77] CMS Collaboration, "Commissioning of the Particle-Flow reconstruction in Minimum-Bias and Jet Events from pp Collisions at 7 TeV", CMS Physics Analysis Summary CMS-PAS-PFT-10-002, 2010.

[78] CMS Collaboration, "Particle-flow commissioning with muons and electrons from J/Psi and W events at 7 TeV", CMS Physics Analysis Summary CMS-PAS-PFT-10-003, 2010.

[79] S. Baffioni et al., "Electron reconstruction in CMS", *Eur.Phys.J.* **C49** (2007) 1099–1116, doi:10.1140/epjc/s10052-006-0175-5.

[80] W. Adam, R. Fruhwirth, A. Strandlie, and T. Todorov, "Reconstruction of electrons with the Gaussian sum filter in the CMS tracker at LHC", *eConf* **C0303241** (2003) TULT009, doi:10.1088/0954-3899/31/9/N01, arXiv:physics/0306087.

[81] CMS Collaboration, "Performance of electron reconstruction and selection with the CMS detector in proton-proton collisions at $\sqrt{s} = 8$ TeV", *JINST* **10** (2015), no. 6, P06005, doi:10.1088/1748-0221/10/06/P06005, arXiv:1502.02701.

[82] CMS Collaboration Collaboration, "Performance of CMS muon reconstruction in pp collision events at $\sqrt{s} = 7$ TeV", *JINST* **7** (2012) P10002, doi:10.1088/1748-0221/7/10/P10002, arXiv:1206.4071.

[83] CMS Collaboration, "Performance of tau-lepton reconstruction and identification in CMS", *JINST* **7** (2012) P01001, doi:10.1088/1748-0221/7/01/P01001, arXiv:1109.6034.

[84] K. Rose, "Deterministic Annealing for Clustering, Compression, Classification, Regression and related Optimisation Problems", *Proceedings of the IEEE* **Vol. 86, Issue 11** (1998).

[85] R. Fruhwirth, W. Waltenberger, and P. Vanlaer, "Adaptive vertex fitting", *J.Phys.* **G34** (2007) N343, doi:10.1088/0954-3899/34/12/N01.

[86] M. Cacciari, G. P. Salam, and G. Soyez, "The anti-k_t jet clustering algorithm", *JHEP* **04** (2008) 063, doi:10.1088/1126-6708/2008/04/063, arXiv:0802.1189.

[87] CMS Collaboration, "Jet Performance in pp Collisions at $\sqrt{s} = 7$ TeV", CMS Physics Analysis Summary CMS-PAS-JME-10-003, 2010.

[88] CMS Collaboration, "Pileup Jet Identification", CMS Physics Analysis Summary CMS-PAS-JME-13-005, 2010.

[89] CMS Collaboration, "Determination of Jet Energy Calibration and Transverse Momentum Resolution in CMS", *JINST* **6** (2011) P11002, doi:10.1088/1748-0221/6/11/P11002, arXiv:1107.4277.

[90] M. Cacciari, G. P. Salam, and G. Soyez, "The Catchment Area of Jets", *JHEP* **0804** (2008) 005, doi:10.1088/1126-6708/2008/04/005, arXiv:0802.1188.

[91] M. Cacciari and G. P. Salam, "Pileup subtraction using jet areas", *Phys. Lett. B* **659** (2008) 119, doi:10.1016/j.physletb.2007.09.077, arXiv:0707.1378.

[92] CMS Collaboration, "Identification of b-quark jets with the CMS experiment", *JINST* **8** (2013) P04013, doi:10.1088/1748-0221/8/04/P04013, arXiv:1211.4462.

[93] CMS Collaboration, "Performance of Missing Transverse Momentum Reconstruction Algorithms in Proton-Proton Collisions at $\sqrt{s} = 8$ TeV with the CMS Detector", CMS Physics Analysis Summary CMS-PAS-JME-12-002, 2012.

[94] L. Bianchini, J. Conway, E. K. Friis, and C. Veelken, "Reconstruction of the Higgs mass in $H \to \tau\tau$ Events by Dynamical Likelihood techniques", *J.Phys.Conf.Ser.* **513** (2014) 022035, doi:10.1088/1742-6596/513/2/022035.

[95] CDF Collaboration Collaboration, "Search for neutral MSSM Higgs bosons decaying to tau pairs in $p\bar{p}$ collisions at $\sqrt{s} = 1.96$ TeV", *Phys.Rev.Lett.* **96** (2006) 011802, doi:10.1103/PhysRevLett.96.011802, arXiv:hep-ex/0508051.

[96] CMS Collaboration, "Electron Reconstruction and Identification at $\sqrt{s} = 7$ TeV", CMS Physics Analysis Summary CMS-PAS-EGM-10-004, 2010.

[97] CMS Collaboration Collaboration, "Measurement of the Inclusive Z Cross Section via Decays to Tau Pairs in pp Collisions at $\sqrt{s} = 7$ TeV", *JHEP* **1108** (2011) 117, doi:10.1007/JHEP08(2011)117, arXiv:1104.1617.

[98] Z. Czyczula, T. Przedzinski, and Z. Was, "TauSpinner Program for Studies on Spin Effect in tau Production at the LHC", *EPJC* **72** (2012) 1988, arXiv:1201.0117.

[99] CMS Collaboration, "Performance of electron reconstruction and selection with the CMS detector in proton-proton collisions at s = 8 TeV", *JINST* **10** (2015), no. 06, P06005, doi:10.1088/1748-0221/10/06/P06005, arXiv:1502.02701.

[100] CMS Collaboration, "Performance of b tagging at $\sqrt{s} = 8$ TeV in multijet, $t\bar{t}$ and boosted topology events", CMS Physics Analysis Summary CMS-PAS-BTV-13-001, 2013.

[101] CMS Collaboration, "Absolute Calibration of the Luminosity Measurement at CMS: Winter 2012 Update", CMS Physics Analysis Summary CMS-PAS-SMP-12-008, 2012.

[102] CMS Collaboration, "CMS Luminosity Based on Pixel Cluster Counting - Summer 2013 Update", CMS Physics Analysis Summary CMS-PAS-LUM-13-001, 2013.

[103] M. Botje et al., "The PDF4LHC Working Group Interim Recommendations", arXiv:1101.0538.

[104] ATLAS Collaboration, "Evidence for the Higgs-boson Yukawa coupling to tau leptons with the ATLAS detector", *JHEP* **1504** (2015) 117, doi:10.1007/JHEP04(2015)117, arXiv:1501.04943.

[105] A. Martin, W. Stirling, R. Thorne, and G. Watt, "Parton distributions for the LHC", *Eur.Phys.J.* **C63** (2009) 189–285, doi:10.1140/epjc/s10052-009-1072-5, arXiv:0901.0002.

[106] A. Martin, W. Stirling, R. Thorne, and G. Watt, "Uncertainties on alpha(S) in global PDF analyses and implications for predicted hadronic cross sections", *Eur.Phys.J.* **C64** (2009) 653–680, doi:10.1140/epjc/s10052-009-1164-2, arXiv:0905.3531.

[107] ATLAS Collaboration, CMS Collaboration and LHC Higgs Combination Group, "Procedure for the LHC Higgs boson search combination in summer 2011", Technical Report ATL-PHYS-PUB-2011-011,CMS-NOTE-2011-005, 2011.

[108] CMS Collaboration Collaboration, "Combined results of searches for the standard model Higgs boson in pp collisions at $\sqrt{s} = 7$ TeV", *Phys.Lett.* **B710** (2012) 26–48, doi:10.1016/j.physletb.2012.02.064, arXiv:1202.1488.

[109] J. Conway, "Incorporating Nuisance Parameters in Likelihoods for Multisource Spectra", arXiv:1103.0354.

[110] R. J. Barlow and C. Beeston, "Fitting using finite Monte Carlo samples", *Comput.Phys.Commun.* **77** (1993) 219–228, doi:10.1016/0010-4655(93)90005-W.

[111] T. Junk, "Confidence level computation for combining searches with small statistics", *Nucl.Instrum.Meth.* **A434** (1999) 435–443, doi:10.1016/S0168-9002(99)00498-2, arXiv:hep-ex/9902006.

[112] A. L. Read, "Presentation of search results: The CL(s) technique", *J.Phys.* **G28** (2002) 2693–2704, doi:10.1088/0954-3899/28/10/313.

[113] A. L. Read, "Linear interpolation of histograms", *Nucl.Instrum.Meth.* **A425** (1999) 357–360, doi:10.1016/S0168-9002(98)01347-3.

[114] ATLAS, CMS Collaboration, "Combined Measurement of the Higgs Boson Mass in pp Collisions at $\sqrt{s} = 7$ and 8 TeV with the ATLAS and CMS Experiments", *Phys.Rev.Lett.* **114** (2015) 191803, doi:10.1103/PhysRevLett.114.191803, arXiv:1503.07589.

[115] CMS Collaboration Collaboration, "Search for charged Higgs bosons with the $H^+ \to \tau^+ \nu_\tau$ decay channel in the fully hadronic final state at $\sqrt{s} = 8$ TeV", *CMS PAS* **HIG-14-020** (2014).

[116] ATLAS Collaboration, "Search for charged Higgs bosons decaying via $H^\pm \to \tau^\pm \nu$ in fully hadronic final states using pp collision data at $\sqrt{s} = 8$ TeV with the ATLAS detector", *JHEP* **1503** (2015) 088, doi:10.1007/JHEP03(2015)088, arXiv:1412.6663.

$e\tau_h$ channel $\sqrt{s} = 7$ TeV		
Process	no-b-tag	b-tag
$gg\phi, \phi \to \tau\tau$	47 ± 2	1 ± 0.1
$bb\phi, \phi \to \tau\tau$	43 ± 2	9 ± 0.6
$Z \to \tau\tau$	11805 ± 349	135 ± 6
QCD	4127 ± 220	78 ± 11
W+jets	1339 ± 130	30 ± 8
Z+jets (e, μ or jet faking τ)	1359 ± 273	9 ± 2
$t\bar{t}$	43 ± 3	20 ± 3
Di-bosons + single top	47 ± 5	7 ± 0.9
SM Higgs	48 ± 14	1 ± 0.1
Total expected	18769 ± 146	280 ± 12
Observed data	18785	274

$e\tau_h$ channel $\sqrt{s} = 8$ TeV			
Process	no-b-tag		
	low	*medium*	*high*
$gg\phi, \phi \to \tau\tau$	57 ± 3	44 ± 3	41 ± 5
$bb\phi, \phi \to \tau\tau$	7 ± 0.4	14 ± 0.7	167 ± 8
$Z \to \tau\tau$	13035 ± 139	1965 ± 63	815 ± 31
QCD	1349 ± 119	194 ± 19	51 ± 7
W+jets	874 ± 119	387 ± 47	290 ± 34
Z+jets (e, μ or jet faking τ)	2027 ± 100	1613 ± 70	380 ± 28
$t\bar{t}$	71 ± 9	30 ± 3	30 ± 5
Di-bosons + single top	59 ± 8	31 ± 5	32 ± 4
SM Higgs	56 ± 17	42 ± 16	19 ± 6
Total expected	17471 ± 133	4261 ± 62	1616 ± 43
Observed data	17457	4291	1604

Process	b-tag	
	low	*high*
$gg\phi, \phi \to \tau\tau$	1 ± 0.1	1 ± 0.2
$bb\phi, \phi \to \tau\tau$	2 ± 0.1	36 ± 2
$Z \to \tau\tau$	156 ± 7	59 ± 3
QCD	26 ± 5	4 ± 0.8
W+jets	20 ± 6	7 ± 3
Z+jets (e, μ or jet faking τ)	14 ± 1	33 ± 2
$t\bar{t}$	24 ± 4	23 ± 4
Di-bosons + single top	7 ± 1	8 ± 1
SM Higgs	1 ± 0.2	1 ± 0.4
Total expected	247 ± 10	134 ± 7
Observed data	260	121

Table 2: Observed and expected event yields in different event categories of the $e\tau_h$ channel. Expected event yields are computed using the values of nuisance parameters obtained by the maximum likelihood fit to the data, described in section 9. Quoted uncertainties represent the combination of statistical plus systematic uncertainties. The signal yield has been computed for the parameter choice $m_A = 350$ GeV and $\tan\beta = 30$ in the $m_h^{\mathrm{mod}+}$ scenario, separately for gluon fusion and b-quark associated production, and refers to the sum of all three neutral MSSM Higgs bosons, $A + H + h$.

$\mu\tau_h$ channel $\sqrt{s} = 7$ TeV		
Process	no-b-tag	b-tag
$gg\phi, \phi \to \tau\tau$	85 ± 4	1 ± 0.1
$bb\phi, \phi \to \tau\tau$	59 ± 3	12 ± 1
$Z \to \tau\tau$	26816 ± 227	283 ± 8
QCD	5423 ± 247	131 ± 17
W+jets	2818 ± 211	57 ± 15
Z+jets (e, μ or jet faking τ)	729 ± 113	11 ± 2
$t\bar{t}$	82 ± 6	38 ± 5
Di-bosons + single top	96 ± 11	13 ± 2
SM Higgs	86 ± 26	1 ± 0.3
Total expected	36050 ± 200	535 ± 17
Observed data	36055	542

$\mu\tau_h$ channel $\sqrt{s} = 8$ TeV			
Process	no-b-tag		
	low	*medium*	*high*
$gg\phi, \phi \to \tau\tau$	122 ± 8	84 ± 6	69 ± 9
$bb\phi, \phi \to \tau\tau$	16 ± 0.7	25 ± 1	250 ± 12
$Z \to \tau\tau$	34836 ± 229	4801 ± 86	1598 ± 46
QCD	1830 ± 159	248 ± 23	94 ± 10
W+jets	2421 ± 207	560 ± 55	357 ± 42
Z+jets (e, μ or jet faking τ)	1219 ± 157	273 ± 50	82 ± 14
$t\bar{t}$	140 ± 17	62 ± 7	58 ± 9
Di-bosons + single top	137 ± 20	69 ± 10	77 ± 11
SM Higgs	122 ± 33	79 ± 21	37 ± 10
Total expected	40706 ± 213	6091 ± 81	2303 ± 48
Observed data	40710	6092	2277

Process	b-tag	
	low	*high*
$gg\phi, \phi \to \tau\tau$	1 ± 0.2	2 ± 0.3
$bb\phi, \phi \to \tau\tau$	3 ± 0.1	51 ± 3
$Z \to \tau\tau$	348 ± 15	140 ± 6
QCD	77 ± 14	11 ± 2
W+jets	37 ± 11	18 ± 7
Z+jets (e, μ or jet faking τ)	6 ± 1	5 ± 0.8
$t\bar{t}$	46 ± 8	47 ± 7
Di-bosons + single top	13 ± 2	14 ± 2
SM Higgs	2 ± 0.4	1 ± 0.3
Total expected	529 ± 17	236 ± 11
Observed data	539	250

Table 3: Observed and expected event yields in different event categories of the $\mu\tau_h$ channel. Expected event yields are computed using the values of nuisance parameters obtained by the maximum likelihood fit to the data, described in section 9. Quoted uncertainties represent the combination of statistical plus systematic uncertainties. The signal yield has been computed for the parameter choice $m_A = 350$ GeV and $\tan\beta = 30$ in the $m_h^{\text{mod}+}$ scenario, separately for gluon fusion and b-quark associated production, and refers to the sum of all three neutral MSSM Higgs bosons, A + H + h.

eμ channel				
Process	$\sqrt{s} = 7$ TeV		$\sqrt{s} = 8$ TeV	
	no-b-tag	b-tag	no-b-tag	b-tag
$gg\phi, \phi \to \tau\tau$	45 ± 2	0 ± 0.1	186 ± 8	2 ± 0.2
$bb\phi, \phi \to \tau\tau$	35 ± 2	8 ± 0.5	177 ± 8	37 ± 2
$Z \to \tau\tau$	13680 ± 141	164 ± 6	48340 ± 313	681 ± 8
QCD	834 ± 119	15 ± 3	4191 ± 368	144 ± 17
$t\bar{t}$	463 ± 29	310 ± 18	2280 ± 175	1188 ± 70
Di-bosons + single top	503 ± 56	64 ± 8	2287 ± 243	294 ± 40
SM Higgs	42 ± 13	1 ± 0.3	165 ± 47	3 ± 1
Total expected	15522 ± 123	554 ± 21	57262 ± 258	2310 ± 66
Observed data	15436	558	57285	2353

Table 4: Observed and expected event yields in different event categories of the eμ channel. Expected event yields are computed using the values of nuisance parameters obtained by the maximum likelihood fit to the data, described in section 9. Quoted uncertainties represent the combination of statistical plus systematic uncertainties. The signal yield has been computed for the parameter choice $m_A = 350$ GeV and $\tan\beta = 30$ in the $m_h^{\text{mod}+}$ scenario, separately for gluon fusion and b-quark associated production, and refers to the sum of all three neutral MSSM Higgs bosons, A + H + h.

μμ channel				
Process	$\sqrt{s} = 7$ TeV		$\sqrt{s} = 8$ TeV)	
	no-b-tag	b-tag	no-b-tag	b-tag
$gg\phi, \phi \to \tau\tau$	21 ± 1	0 ± 0.1	74 ± 4	0 ± 0.1
$bb\phi, \phi \to \tau\tau$	19 ± 0.9	3 ± 0.1	88 ± 5	14 ± 0.9
$Z \to \tau\tau$	7066 ± 154	35 ± 2	20369 ± 428	99 ± 5
$Z \to \mu\mu$	561809 ± 784	1435 ± 33	1894920 ± 1531	5139 ± 74
QCD	375 ± 55	4 ± 2	1142 ± 108	31 ± 7
$t\bar{t}$	186 ± 17	84 ± 8	842 ± 85	322 ± 33
Di-bosons + single top	1109 ± 215	10 ± 2	5630 ± 840	47 ± 9
SM Higgs	21 ± 7	0 ± 0.1	74 ± 24	1 ± 0.2
Total expected	570566 ± 792	1567 ± 35	1922977 ± 1405	5638 ± 74
Observed data	570616	1559	1922924	5608

Table 5: Observed and expected event yields in different event categories of the μμ channel. Expected event yields are computed using the values of nuisance parameters obtained by the maximum likelihood fit to the data, described in section 9. Quoted uncertainties represent the combination of statistical plus systematic uncertainties. The signal yield has been computed for the parameter choice $m_A = 350$ GeV and $\tan\beta = 30$ in the $m_h^{\text{mod}+}$ scenario, separately for gluon fusion and b-quark associated production, and refers to the sum of all three neutral MSSM Higgs bosons, A + H + h.

$\tau_h\tau_h$ channel $\sqrt{s} = 8$ TeV			
Process	no-b-tag		
	low	*medium*	*high*
$gg\phi, \phi \to \tau\tau$	66 ± 8	23 ± 5	28 ± 3
$bb\phi, \phi \to \tau\tau$	82 ± 8	108 ± 10	174 ± 18
$Z \to \tau\tau$	1645 ± 73	542 ± 34	193 ± 13
QCD	6982 ± 144	942 ± 52	147 ± 21
W+jets	428 ± 116	122 ± 38	28 ± 9
Z+jets (e, μ or jet faking τ)	65 ± 10	23 ± 3	5 ± 0.9
$t\bar{t}$	23 ± 3	8 ± 1	2 ± 0.4
Di-bosons + single top	37 ± 8	16 ± 3	6 ± 1
SM Higgs	48 ± 16	8 ± 2	2 ± 0.6
Total expected	9228 ± 98	1659 ± 44	382 ± 22
Observed data	9259	1695	400

Process	b-tag	
	low	*high*
$gg\phi, \phi \to \tau\tau$	1 ± 0.3	1 ± 0.1
$bb\phi, \phi \to \tau\tau$	18 ± 2	58 ± 8
$Z \to \tau\tau$	35 ± 3	14 ± 2
QCD	118 ± 11	21 ± 4
W+jets	6 ± 2	2 ± 1
Z+jets (e, μ or jet faking τ)	1 ± 0.2	0 ± 0.1
$t\bar{t}$	9 ± 2	5 ± 0.9
Di-bosons + single top	2 ± 0.5	3 ± 0.6
SM Higgs	1 ± 0.3	0 ± 0.1
Total expected	172 ± 11	45 ± 5
Observed data	172	41

Table 6: Observed and expected event yields in different event categories of the $\tau_h\tau_h$ channel. Expected event yields are computed using the values of nuisance parameters obtained by the maximum likelihood fit to the data, described in section 9. Quoted uncertainties represent the combination of statistical plus systematic uncertainties. The signal yield has been computed for the parameter choice $m_A = 350$ GeV and $\tan\beta = 30$ in the $m_h^{\mathrm{mod}+}$ scenario, separately for gluon fusion and b-quark associated production, and refers to the sum of all three neutral MSSM Higgs bosons, A + H + h.

Parameter	$m_{\mathrm{h}}^{\mathrm{max}}$	$m_{\mathrm{h}}^{\mathrm{mod+}}$	$m_{\mathrm{h}}^{\mathrm{mod-}}$
m_{A}	90–1000 GeV	90–1000 GeV	90–1000 GeV
$\tan\beta$	0.5–60	0.5–60	0.5–60
M_{SUSY}	1000 GeV	1000 GeV	1000 GeV
μ	200 GeV	200 GeV	200 GeV
M_1	$(5/3)\, M_2 \tan^2\theta_W$	$(5/3)\, M_2 \tan^2\theta_W$	$(5/3)\, M_2 \tan^2\theta_W$
M_2	200 GeV	200 GeV	200 GeV
X_t	2 M_{SUSY}	1.5 M_{SUSY}	-1.9 M_{SUSY}
A_b, A_τ	$A_b = A_\tau = A_t$	$A_b = A_\tau = A_t$	$A_b = A_\tau = A_t$
$m_{\tilde{\mathrm{g}}}$	1500 GeV	1500 GeV	1500 GeV
$m_{\tilde{\mathrm{l}}_3}$	1000 GeV	1000 GeV	1000 GeV

Parameter	light-stop	light-stau	τ-phobic	low-m_{H}
m_{A}	90–600 GeV	90–1000 GeV	90–1000 GeV	110 GeV
$\tan\beta$	0.7–60	0.5–60	0.9–50	1.5–9.5
M_{SUSY}	500 GeV	1000 GeV	1500 GeV	1500 GeV
μ	400 GeV	500 GeV	2000 GeV	300-3100 GeV
M_1	340 GeV	$(5/3)\, M_2 \tan^2\theta_W$	$(5/3)\, M_2 \tan^2\theta_W$	$(5/3)\, M_2 \tan^2\theta_W$
M_2	400 GeV	200 GeV	200 GeV	200 GeV
X_t	2 M_{SUSY}	1.6 M_{SUSY}	2.45 M_{SUSY}	2.45 M_{SUSY}
A_b, A_τ	$A_b = A_\tau = A_t$	$A_b = A_t, A_\tau = 0$	$A_b = A_\tau = A_t$	$A_b = A_\tau = A_t$
$m_{\tilde{\mathrm{g}}}$	1500 GeV	1500 GeV	1500 GeV	1500 GeV
$m_{\tilde{l}_3}$	1000 GeV	245 GeV	500 GeV	1000 GeV

Table 7: MSSM benchmark scenarios. M_{SUSY} denotes the common soft-SUSY-breaking third-generation squark masses; μ the higgsino mass parameter; M_1 (M_2) the $U(1)$ ($SU(2)$) gaugino mass parameter; X_t the stop mixing parameter; A_t, A_b and A_τ are the trilinear Higgs–stop, Higgs–sbottom and Higgs–stau-lepton couplings, respectively; $m_{\tilde{\mathrm{g}}}$ ($m_{\tilde{l}_3}$) the gluino (third generation slepton) mass. A_t is given by the relation $A_t = X_t + \mu/\tan\beta$. The parameter θ_w denotes the weak mixing angle, given by $\cos\theta_w = m_{\mathrm{W}}/m_{\mathrm{Z}}$.